**Forschungszentrum Karlsruhe**
in der Helmholtz-Gemeinschaft

**Wissenschaftliche Berichte**
FZKA 6931

# Creep-fatigue Lifetime Prediction Rules for Ferritic Martensitic Steels

## (Final Report, Task: TW2-TTMS-005a, D4)

**J. Aktaa, R. Schmitt**

**Institut für Materialforschung**
**Programm Kernfusion**
**Association Forschungszentrum Karlsruhe/EURATOM**

**Mai 2004**

**Forschungszentrum Karlsruhe**

in der Helmholtz-Gemeinschaft

Wissenschaftliche Berichte

FZKA 6931

# Creep-fatigue lifetime prediction rules for Ferritic Martensitic Steels

(Final Report, Task: TW2-TTMS-005a, D4)

Jarir Aktaa and Rolf Schmitt

Institut für Materialforschung

Programm Kernfusion

Association Forschungszentrum Karlsruhe/EURATOM

Forschungszentrum Karlsruhe GmbH, Karlsruhe

2004

**Impressum der Print-Ausgabe:**

**Als Manuskript gedruckt**


**Forschungszentrum Karlsruhe GmbH**
**Postfach 3640, 76021 Karlsruhe**

**Mitglied der Hermann von Helmholtz-Gemeinschaft**
**Deutscher Forschungszentren (HGF)**

**ISSN 0947-8620**

**urn:nbn:de:0005-069318**

**Abstract**

Structural materials of fusion reactors are subjected to complex creep-fatigue loading and high irradiation doses. Correct modelling of their deterioration is a precondition of a sufficiently reliable lifetime prediction procedure.

In the continuum mechanics approach selected for lifetime prediction of RAFM steels under creep-fatigue conditions the ISRM (Inelastic Strain Rate Modified) damage model is coupled with a modified viscoplastic deformation model taking into account the complex non-saturating cyclic softening of RAFM steels. The resulting coupled model is a powerful prediction tool, which can be applied to arbitrary creep-fatigue loading provided that the material, temperature and possibly irradiation dose dependent parameters of the model have been determined. Therefore a fitting procedure has been developed for the parameters identification on the base of deformation and lifetime data from standard low cycle fatigue (LCF) tests without and with hold time as well as creep tests.

The coupled deformation-damage model has been meanwhile applied to F82H mod and EUROFER 97 in the reference (unirradiated) state under isothermal cyclic loading at 450, 550 and 650 °C. The comparisons between model and experiment show that the observed lifetimes in the LCF-tests could be fairly well calculated even for the tests with hold time, which were not considered for the identification of the damage model parameters. However before releasing the model further verifications have to be done by applying the model to isothermal two-steps LCF-tests (low-to-high and high-to-low), to thermo-mechanical LCF-tests, to isothermal multiaxial LCF-tests as well as to a suitable benchmark component test. To take into account the influence of irradiation applications of the model are in long term foreseen to several irradiated states with sufficient data base.

**Zusammenfassung**

**Lebensdauermodellierung ferritsch-martensitischer Stähle**

Die Strukturwerkstoffe von Fusionsreaktoren unterliegen im geplanten Betrieb komplexen Kriechermüdungs- und hohen Bestrahlungsbelastungen. Die korrekte Modellierung ihrer Schädigung bei diesen Belastungen ist eine Voraussetzung für eine hinreichend zuverlässige Lebensdauervorhersage.

Zur Beschreibung der Schädigung ferritisch-martensitischer Stähle bei einer Kriechermüdungsbelastung wurde im Rahmen eines kontinuummechanischen Konzepts das ISRM-Modell (Inelastic Strain Rate Modified) mit einem modifizierten viskoplastischen Verformungsmodell gekoppelt. Damit lassen sich das komplexe zyklische Entfestigungsverhalten dieser Stähle sowie die Wechselwirkung zwischen Verformung und Schädigung bei der Berechnung der Lebensdauer berücksichtigen. Das resultierende gekoppelte Modell ist auf beliebige Kriech-Ermüdungsbelastungen anwendbar. Für die Anwendung müssen allerdings die darin enthaltenen material-, temperatur- und bestrahlungsdosisabhängigen Parameter bestimmt werden. Für diesen Zweck wurde eine Anpassungsmethode entwickelt, mit der die Parameterbestimmung auf der Basis von Daten aus standardisierten Kriech- und LCF-Versuchen ohne und mit Haltezeit erfolgen kann.

Das gekoppelte Verformungs-Schädigungs-Modell wurde mittlerweile auf F82H-mod und EUROFER 97 jeweils in dem unbestrahlten Anlieferzustand angewandt. Betrachtet wurden dabei isotherme LCF-Versuche bei 450, 550 und im Falle F82H mod auch 650°C. Der Vergleich zwischen Modell und Experiment zeigt, dass die im Experiment ermittelten Lebensdauern recht gut durch das Modell wiedergegeben werden. Auch bei der Vorhersage der Lebensdauern von LCF-Versuchen mit Haltezeit, die für die Bestimmung der Parameter des Schädigungsmodells nicht herangezogen wurden, liefert das Modell gute Ergebnisse. Entsprechendes konnte auch für EUROFER 97 erzielt werden. Für die Anwendung des Modells auf reale Strukturen mit reaktortypischen Belastungen sind jedoch weitere Verifikationen notwendig, bei denen isotherme zweistufige (tief-hoch und hoch-tief), thermomechanische einachsige und isotherme mehrachsige LCF-Versuche sowie geeignete Bauteilversuche betrachtet werden. Um den Bestrahlungseinfluss zu berücksichtigen, sind langfristig auch Anwendungen auf mehrere bestrahlte Zustände mit hinreichender Datenbasis vorgesehen.

## CONTENTS

# 1 Introduction

Reduced activation ferritic martensitic (RAFM) steels developed recently inter alia in the framework of EURATOM Fusion Technology programme are potential candidate for structural materials of future fusion reactors [1]. Within our activities in the EFDA Technology Work programme with the reference TTMS-005 “RAFM Steels: Rules for Design, Fabrication and Inspection” lifetime prediction rules for RAFM steels will be developed and qualified for a design code.

During planed operation of a fusion reactor structural materials of the plasma facing components, Blanket and Divertor, are subjected to complex thermo-mechanical loading and high irradiation doses which induce different kinds of damage: creep, fatigue as well as irradiation damage [2] [3]. Since all these damage types appear together they may influence each other and thus their evolutions can not be considered separately. Lifetime prediction laws in appropriate design codes used by designer for analysing and dimensioning of components shall take this into account.

In our concept we started developing a lifetime prediction model for RAFM steels under creep and fatigue conditions taking into account the creep fatigue interaction. The model consists of a damage model coupled with a deformation model. The coupling allows on the one hand the consideration of mutual influence between deformation and damage and on the other hand the lifetime prediction for an arbitrary loading without the need of additional strain or stress measurements. Both, the deformation and the damage model were developed within the framework the continuum mechanics using the phenomenological concept of state variables to describe complex irreversible processes like plastic deformation and damage. In addition the models were formulated in a way that they can be implemented in commercial Finite Element codes and thus be used for the assessment of arbitrary shaped components.

The development of the deformation and damage models has been based on the identification of important mechanisms influencing damage evolution and thus the lifetime. Therefore the experimental observations, in particular those obtained from isothermal low cycle fatigue tests were deeply analysed. The main outcome of this analysis is discussed in the first section of this report. In the following sections the models and the results of their application on most promising candidates of RAFM steels, F82H mod and EUROFER 97, are presented.

# 2 Experimental observations

Since damage evolution under combined creep and fatigue loading is of main interest the experimental results obtained from isothermal low cycle fatigue test on F82H mod and EUROFER 97 have been considered. Both materials behave qualitatively similar so that the phenomena discussed below for the one material are also valid for the other and vice versa.

Stress is one of the major factors influencing damage whereas small changes in stress lead to super proportional changes in damage evolution and lifetime, respectively. Fig. 2-1 show for four strain controlled LCF tests  the change of peak stress versus the number of cycles

$N$ normalized by the number of cycles to failure $N_f$ obtained in the respective test. In a closer look to the curves the following can be noticed:

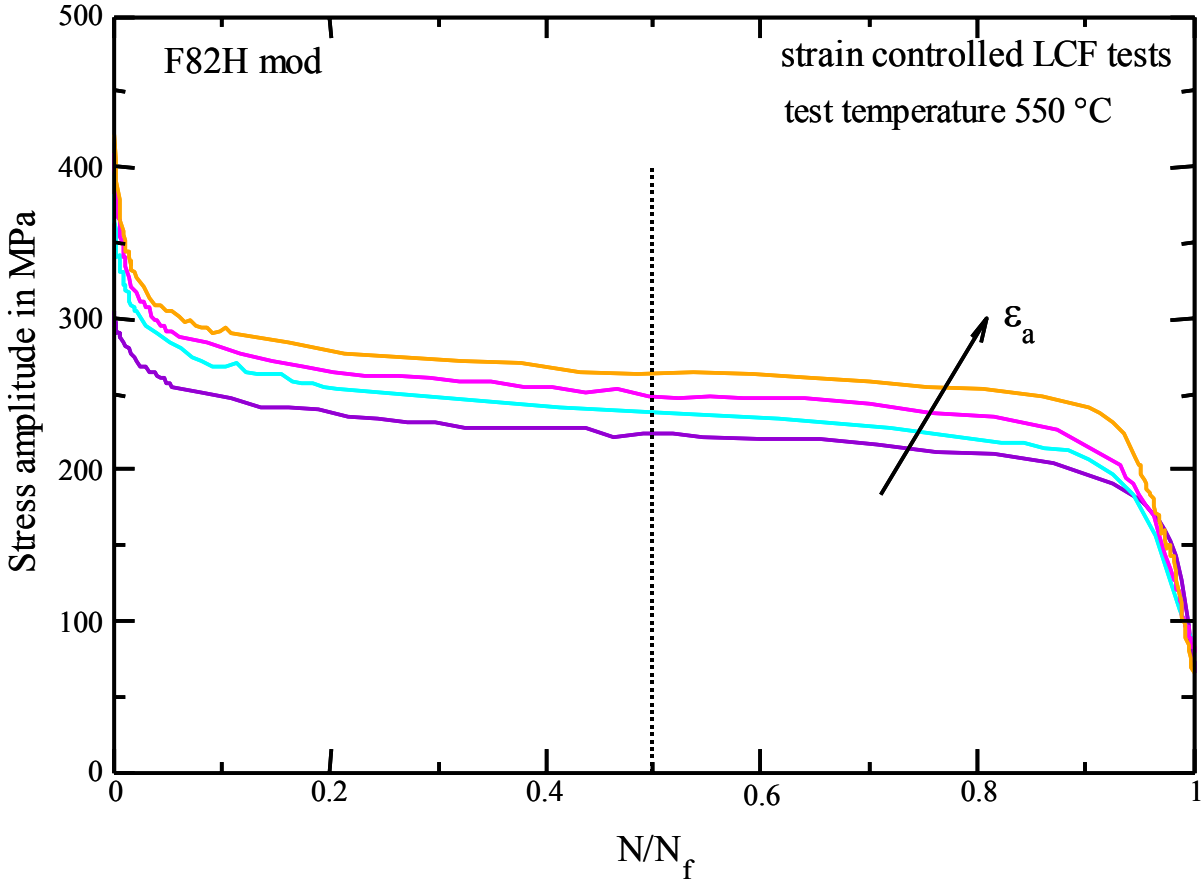


Fig. 2-1 Stress amplitude versus normalized number of cycles for strain controlled LCF tests with different strain amplitudes

1. The RAFM steels, here represented by F82H mod, exhibit cyclic softening which is very strong in the first cycles leading to a decrease in the strength up to 30 % of the initial strength value within the first 0.1 part of the lifetime. This is very important and has to be taken into account particularly when using strength data produced in tensile and creep tests on non-cycled material for the dimensioning and assessment of cyclically loaded structures.

2. In the main middle part of the lifetime the cyclic softening becomes slower with more or less constant slope over the normalized number of cycles. That means there is no stop of the cyclic softening and consequently there is no saturation cycle which can be considered as a representative cycle for this period of lifetime. Therefore numerous lifetime prediction rules, like Manson-Coffin for instance, which need as input the loading within a representative cycle can not be applied without an additional criteria. The selection of the cycle at $N_f/2$ as a representative cycle could such a criteria which makes no sense in the case of lifetime prediction where $N_f$ is unknown.

3. In the last 0.2 part of the lifetime an acceleration of the cyclic softening occurs caused by damage which becomes high enough so that its influence on the deformation behaviour gets recognizable. The acceleration can actually be interpreted as a measure for damage evolution. Accordingly the damage evolution seems to be similar for all four tests considered, i.e. independent on the loading level. Therefore the damage accumulation under variable loading is expected be linear which has to be verified in suitable experiments.

The damage behaviour becomes more complicated when inserting a hold time period within the cycle of the high temperature LCF test. Such a hold time period simulates the loading of a component under stationary operation. During the hold time period additional creep damage is expected which might shorten the lifetime remarkably. When considering the strain controlled LCF tests with different hold times under tension in comparison to each other and to the test without hold time (s. Fig. 2-2) the following can be observed:

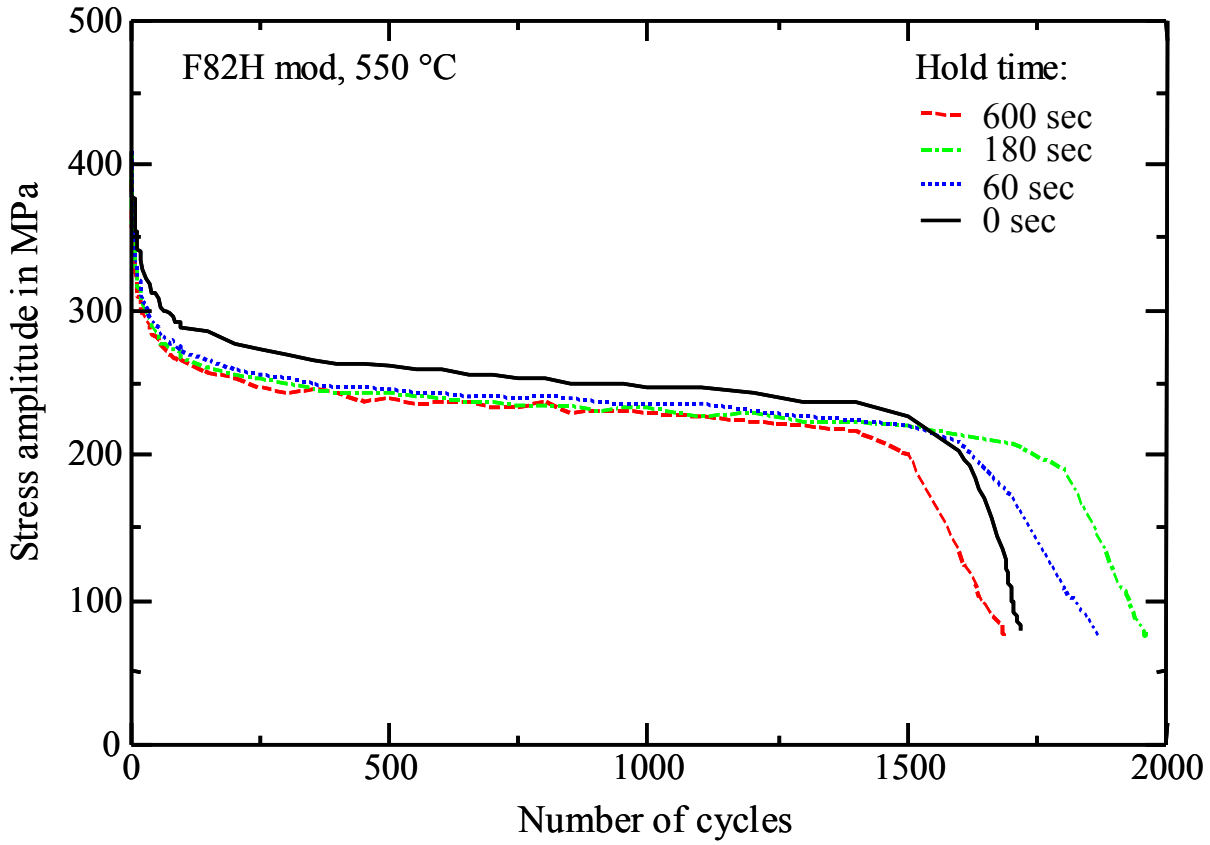


Fig. 2-2 Stress amplitude versus number of cycles for strain controlled LCF tests with different hold times under tension

1. Due to the hold time period additional cyclic softening occurs which might be explained by the additional inelastic strain appearing during the hold time period and resulting in stress relaxation. With longer hold times the additional cyclic softening increases but -- like the stress relaxation within a cycle – not as much as it does short hold times.

2. In spite of the additional creep damage and the increase inelastic strain range due to the hold time within a cycle short hold times extend the cyclic lifetime which can be explained by the peak stress reduction due to the additional cyclic softening. However, with longer hold time period creep damage increases and its shortening influence on the cyclic lifetime overcomes the extending influence of the additional cyclic softening, like it is the case for the LCF test with 600 sec hold time in Fig. 2-2.

3. In a closer look to the stress relaxation during the hold time period a reduction of its amount is recognised as a results of the cyclic softening, i.e. not only the strength of the material but also its viscosity are reduced by the cyclic softening, up to 60% for the test considered in Fig. 2-3.

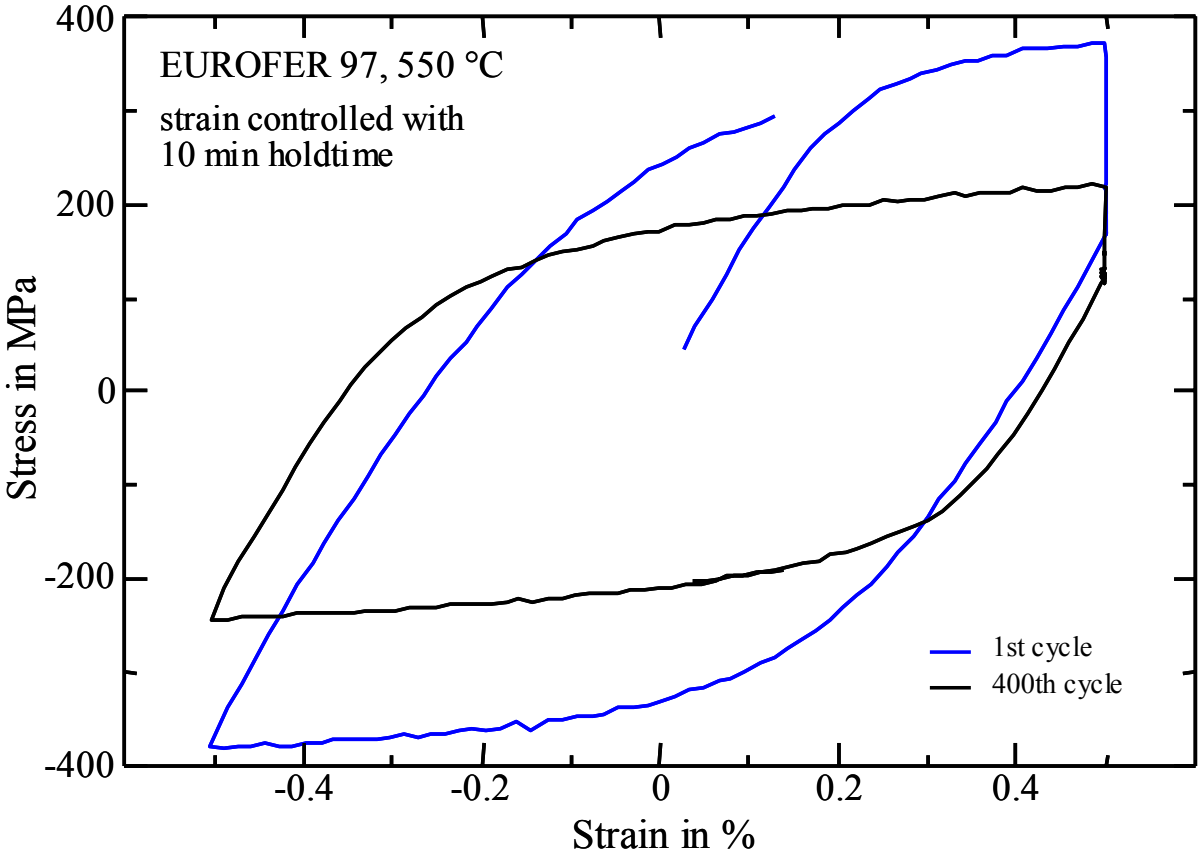


Fig. 2-3 Stress strain hysteresis loops for the 1st and 400th cycle of a strain controlled LCF tests with hold time under tension. The influence of cyclic softening on the peak stress as well on the stress relaxation and viscosity, respectively, can be noticed.

When inserting the hold time period under compression or under tension and compression, respectively, the damage and lifetime behaviour is totally different from that what is expected on the base of the experience with the majority of metallic materials. So hold time under compression ends with a shorter lifetime in comparison to the hold time under tension or even to hold time under tension and compression, respectively (s. Fig 2-4). This is surprising because during the lifetime under compression no creep damage or much less than under

tension can be physically initiated. However, a closer look to the stress and strain data of the strain controlled LCF test allows at least qualitatively an explanation for this strange behaviour:

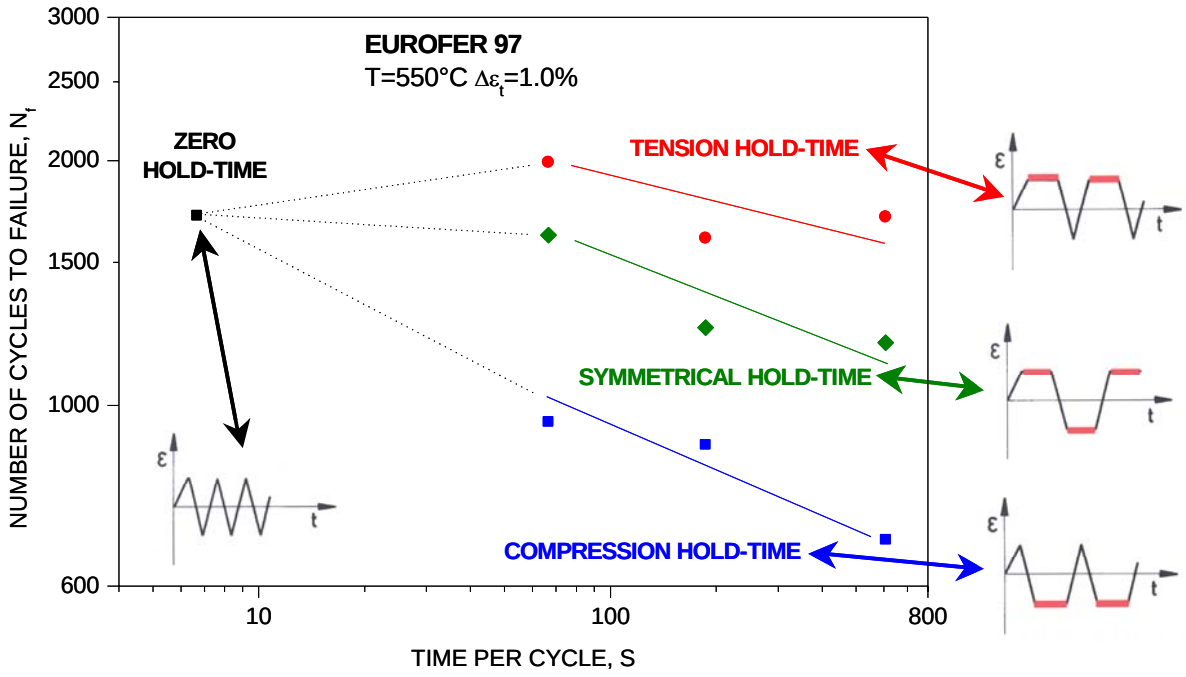


Fig. 2-4 Influence of hold time duration and position on the number of cycles to failure of strain controlled LCF tests

1. Fig. 2-5 shows the stress strain hysteresis loops at the half of the lifetime $N_f/2$ for the tests with hold time under tension and with hold time under compression, respectively. It can be noticed that the inelastic strain ranges for the test with hold time under compression and the test with hold time under tension are equal. So the inelastic strain range can not be the only factor determining the lifetime like it is assumed by some lifetime prediction rules. However, hold time under compression does not cause a reduction of the tensile peak stress like hold time under tension does. This would explain the stronger negative influence of the hold time under compression on the lifetime.

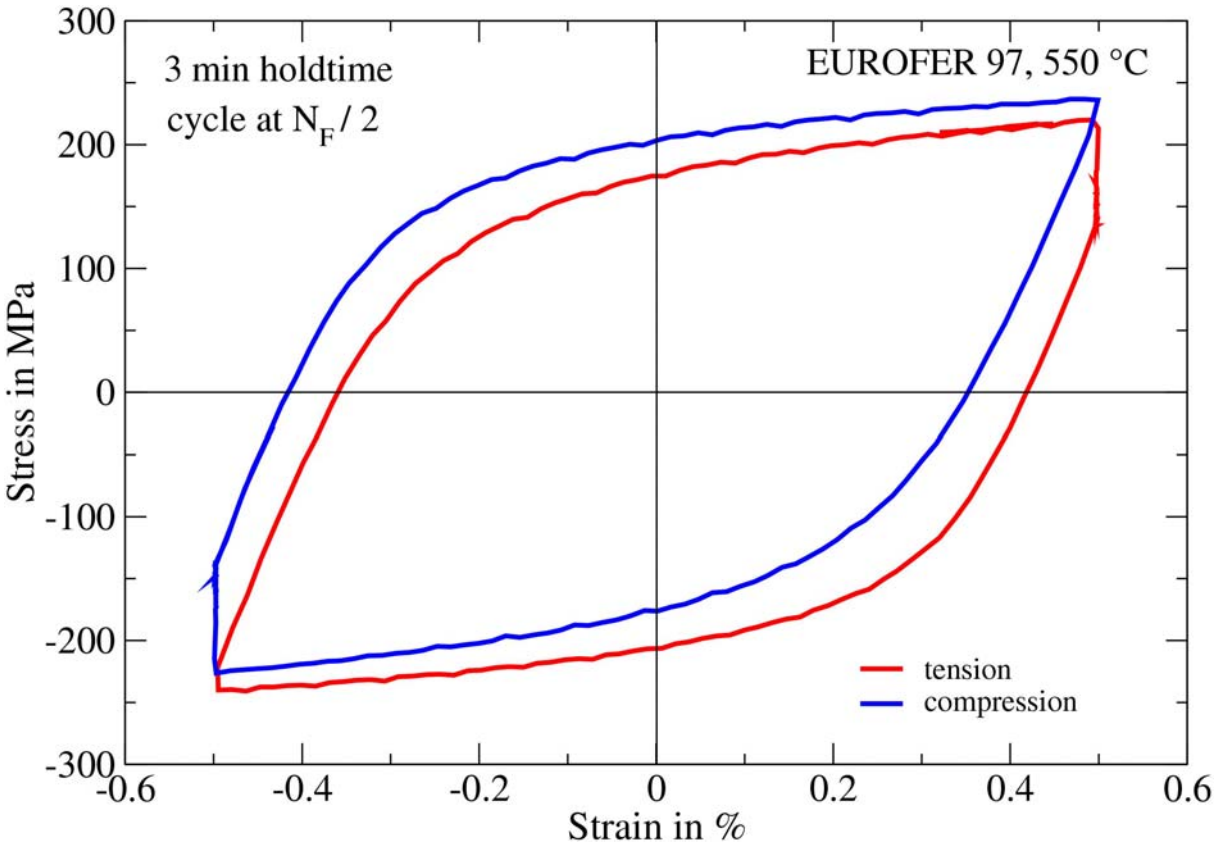


Fig. 2-5 Stress strain hysteresis loops at the half of the lifetime $N_f / 2$ for the tests with hold time under tension and with hold time under compression, respectively

2. To find an explanation why the test with hold times under tension and compression, respectively, yields to a longer lifetime in comparison to the test with hold time under compression only we plotted the respective stress strain hysteresis loops at $N_f / 2$ in Fig. 2-6. Also here it can be noticed that the tensile peak stress for the test with hold times under tension and compression, respectively is lower than that for the test with hold time under compression and actually as low as that for the test with hold time under tension (cf. Fig. 2-5 and Fig. 2-6). However, it seems that the tensile peak stress for the test with hold times under tension and compression, respectively, is low enough so that its negative influence on the lifetime is strongly reduced compensating the damaging influence of the higher inelastic strain range and of the additional creep during the tensile hold time. By the way, the higher inelastic strain range (cf. Fig. 2-5 and Fig. 2-6) would explain why the test with hold times under tension and compression, respectively, has the lower cyclic lifetime than the test with hold time under tension.

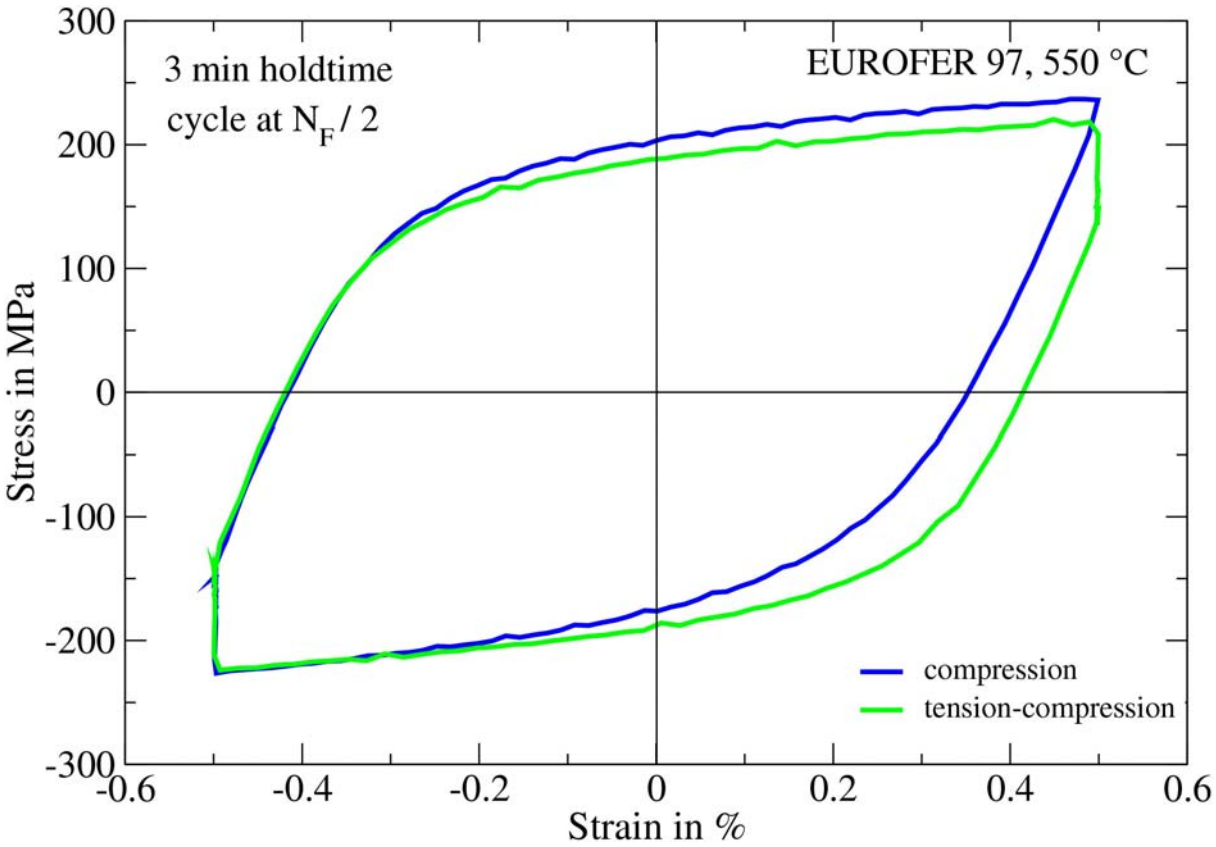


Fig. 2-6 Stress strain hysteresis loops at the half of the lifetime $N_f / 2$ for the tests with hold time under compression and with hold time under tension and compression, respectively

All the insights illustrated above build the base of the selection and modification of the suitable deformation and damage models for the description of the mechanical behaviour of RAFM steels.

# 3 Coupled deformation damage model

The analysis of the experimental observations showed, that damage and lifetime are not only dependent on the applied loading but also on the deformation response of the material to this loading. The prediction of the deformation response is a precondition for a reliable description of the resulting damage evolution and lifetime behaviour, respectively. Thus, the approach we adopted starts with the selection of a deformation model suitable to describe the deformation behaviour of the undamaged material and then the coupling with a damage model to describe the behaviour up to failure ending with the lifetime prediction. Failure of a material point is defined by the macro crack initiation at that point, i.e. the lifetime covers the time needed for micro crack initiation and micro crack propagation up to macro crack. In the following the deformation, damage and the coupled model are presented in their uniaxial formulation for simplification. The multiaxial formulation of the coupled model can be found in Appendix A.

## 3.1 Deformation model

To describe the elasto-viscoplastic deformation behaviour of RAFM steels a model is proposed based on the model by Chaboche [4] which has been modified to include the complex cyclic softening behaviour of RAFM mentioned in the previous section. The model belongs to the so called unified deformation models which describe viscoplasticity without the separation in time dependent creep and time independent plasticity [5]. Consequently, the total strain rate is subdivided in an elastic, inelastic and thermal parts:

$$\dot{\varepsilon} = \dot{\varepsilon}^{el} + \dot{\varepsilon}^{in} + \dot{\varepsilon}^{th} \tag{3.1}$$

The thermal strain is determined using the coefficient of thermal expansion $\alpha$

$$\varepsilon^{th} = \alpha\ (\mathrm{T} - \mathrm{T}_0) \tag{3.2}$$

with $T$ denoting the temperature whereas the elastic strain is calculated using the Hook's law

$$\varepsilon^{el} = \frac{\sigma}{E} \tag{3.3}$$

with $\sigma$ and $E$ denoting the stress and the Young modulus, respectively. For the inelastic strain a flow rule is formulated where the inelastic strain rate is given as a function of the observable state variables, stress and temperature, as well as of the internal state variable $\Omega$ and $\psi$ describing the kinematic hardening and the isotropic softening, respectively:

$$\dot{\varepsilon}^{in} = \left\langle \frac{|\Sigma| - k}{Z} \right\rangle^{n} \mathrm{sgn}(\Sigma) \qquad \text{with} \qquad \Sigma = \frac{\sigma}{\psi} - \Omega \tag{3.4}$$

The brackets $\langle\ \rangle$ operates on the term in between as follows: $\langle \mathrm{x} \rangle = (\mathrm{x} + |\mathrm{x}|)/2$. The nonlinear change of the kinematic hardening is described by the appropriate evolution equation:

$$\dot{\Omega} = H\dot{\varepsilon}^{in} - D\Omega\left|\dot{\varepsilon}^{in}\right| - R|\Omega|^{m-1}\Omega \tag{3.5}$$

The isotropic softening variable $\psi$ is subdivided in two parts $\psi_1$ and $\psi_2$ with

$$\psi = \psi_1 + \psi_2 \qquad \text{with} \qquad \psi_1\,(\mathrm{t}=0) = 0 \qquad \text{and} \qquad \psi_2\,(\mathrm{t}=0) = 1 \tag{3.6}$$

The change of each part of the isotropic softening is given by a separate evolution equation:

$$\dot{\psi}_1 = -h\left|\dot{\varepsilon}^{in}\right| \tag{3.7}$$

$$\dot{\psi}_2 = c\ (\psi_s - \psi_2)\left|\dot{\varepsilon}^{in}\right| - r_{\psi}\left|\psi_2 - \psi_r\right|^{m_{\psi}-1}(\psi_2 - \psi_r)$$

$$\text{with} \qquad \psi_s = 1 - \psi_{s,\infty}\left(1 - \exp\left(-c_s \max_{-\infty<\tau<t}\left|\varepsilon^{in}(\tau)\right|\right)\right) \tag{3.8}$$

$\psi_1$ and $\psi_2$ allow the description of the non saturating part and the initial non-linear part of the cyclic softening, respectively. With $\psi_s$ the memorised increase of the cyclic softening capacity with increasing inelastic strain amplitude is included. The last terms in eq. 3.5 and 3.8 represent static recoveries of the kinematic hardening and the isotropic softening, respectively, which might be observed under creep, relaxation or cyclic loading with hold time.
$k$, $Z$, $n$, $H$, $D$, $R$, $m$, $h$, $c$, $r_\psi$, $\psi_r$, $m_\psi$, $\psi_{s,\infty}$ and $c_s$ are like the Young modulus $E$ and the coefficient of thermal expansion $\alpha$ material, temperature and possibly irradiation dose dependent parameters. They have to be determined by fitting the model to the material deformation behaviour observed experimentally.

## 3.2 Damage model

To describe damage a model has been selected which is a simplified version of the ISRM (inelastic strain rate modified) model by Aktaa and Schinke [6]. The simplification is based on the assumption that damage accumulates linearly under variable loading what is suspected when analysing the experimental observations (s. previous section). The ISRM model was successfully applied to numerous metallic alloys used at high temperatures [6], among others those in the post irradiated state [7]. It is capable to describe creep, fatigue as well as creep-fatigue interaction. It was developed within the framework of continuum damage mechanics by introducing an internal state variable $\mathrm{D}$ for damage with values range between 0 for virgin material and 1 for totally damaged material [8]. In the simplified ISRM model the change of $\mathrm{D}$ is described by the following evolution equation [7]

$$\dot{\mathrm{D}} = \left\langle \frac{\sigma}{A} \right\rangle^r \left| \dot{\varepsilon}^{in} \right| \left(1 - \mathrm{D}\right)^{-\kappa} \tag{3.9}$$

with $A$, $r$ and $\kappa$ as material, temperature and irradiation dose dependent parameters. With the brackets $\langle\ \rangle$ no damage change is assumed under compression. In addition damage remains constant if the material does not undergo inelastic deformation.

## 3.3 Coupled model

The continuum damage mechanics approach allows the coupling between deformation and damage simply by replacing the stress $\sigma$ in the deformation model by the so called effective stress $\tilde{\sigma}$ [9],

$$\tilde{\sigma} = \frac{\sigma}{1 - \mathrm{D}} \quad , \tag{3.10}$$

particularly in eq. 3.3 and 3.4 leading to

$$\varepsilon^{el} = \frac{\sigma}{E(1 - \mathrm{D})} \tag{3.11}$$

and

$$\dot{\varepsilon}^{in} = \left\langle \frac{|\Sigma| - k}{Z} \right\rangle^{n} \operatorname{sgn}(\Sigma) \qquad \text{with} \qquad \Sigma = \frac{\sigma}{\psi(1-D)} - \Omega \tag{3.12}$$

# 4 Application of coupled deformation damage model to RAFM steels

The application of the coupled deformation damage model presented in the previous section for lifetime prediction require the determination of the material, temperature and irradiation dose dependent parameters. Because of their high number the parameters can not be determined simultaneously and an appropriate fitting strategy is needed.

## 4.1 Determination of model parameters

The strategy used considers the correlations between the parameters and separates them in subsets with the parameters in each subset correlating so strong with each other that they can not be determined separately. On the other hand material data sets suitable for the determination of the different parameters subsets are selected from the data base available for the material. Thereafter a stepwise identification of the parameters subsets is performed by minimizing the error between model and material response whereas the following error function is used [10]

$$\chi^2 = \sum_{m=1}^{n_{\exp}} \sum_{n=1}^{n_{dat,m}} \left( \frac{\sigma_{mn}^{model} - \sigma_{mn}^{experiment}}{n_{dat,m}} \right)^2 \tag{4.1}$$

with $n_{\exp}$ as the number of experiments in each material data set and $n_{dat,m}$ as the number of data points considered from the experiment $m$. For the minimization of this function the optimisation code MINUIT from the CERNLIB is used.

For our application the data base consists of deformation and lifetime data of isothermal strain controlled low cycle fatigue (LCF) tests without and with hold times as well as of isothermal creep tests. According to experience this data base is not necessarily the best for the parameters identification but it is sufficient. However the parameters identification has been performed according the strategy described above in the following order:

**Step 1.** The parameters $k$, $Z$, $n$, $H$ and $D$ are determined by fitting the model response to the stress strain curve of the first cycles of the LCF tests without and with hold time and fixing the other parameters at negligible values.

**Step 2.** The parameters $k$, $Z$, $n$, $H$ and $D$ are fixed at their in step 1 optimised values and from the remaining parameters only $R$ and $m$ are released to be determined by fitting the model response to the stationary creep rates data

**Step 3.** The parameters $R$ and $m$ are fixed at their in step 2 optimised values and from the remaining parameters only $h$, $c$, $\psi_{s,\infty}$ and $c_s$ are released to be determined by fitting the model response to the cyclic softening curves (peak stress vs. number of cycles) of the LCF tests without hold time up to the half of the number of cycles to failure.

**Step 4.** The parameters $h$, $c$, $\psi_{s,\infty}$ and $c_s$ are fixed at their in step 3 optimised values and from the remaining parameters only $r_\psi$, $\psi_r$ and $m_\psi$ are released to be determined by fitting the model response to the cyclic softening curves (peak stress vs. number of cycles) of the LCF tests with hold time up to the half of the number of cycles to failure.

**Step 5.** The parameters $r_\psi$, $\psi_r$ and $m_\psi$ are fixed at their in step 4 optimised values and from the remaining parameters only $A$, $r$ and $\kappa$ are released to be determined by fitting the model response to the cyclic softening curves (peak stress vs. number of cycles) of the LCF tests without hold time up to the number of cycles to failure.

In each of the fitting steps illustrated above the parameters to be determined obtain at the beginning initial values estimated on the base of experience and first assessments of the material data.

## 4.2 Results

Applying the parameters determination procedure presented in the previous subsection parameters sets are determined for F82H mod at 450, 550 and 650 °C and EUROFER 97 at 450 and 550 °C. The parameters sets are listed in Appendix B, respectively.

The quality of the fits are demonstrated using comparisons between model responses after the fits with those of the material. In Fig. 4-1 it can be recognized that the stress/strain behaviour in the first cycles of LCF tests performed with different total strain ranges are fairly well described by the model. The complex cyclic softening behaviour is also well described by the model as it is demonstrated exemplarily in Fig. 4-2. Similar comparisons for the other LCF tests are collected in Appendix C. Good agreements between model and experiment could also be achieved for the damage (lifetime) behaviour (Figs. 4-3 and 4-4). The differences between fatigue lifetimes calculated and experimentally observed lie within a range of factor two except for only tests with a lifetime lying in the transition range to high cycle fatigue (s. Fig. 4-4). In the high cycle fatigue regime, the ISRM damage model is expected to underestimate the lifetime what has been found also in former studies [11] and is however a conservative safe prediction.

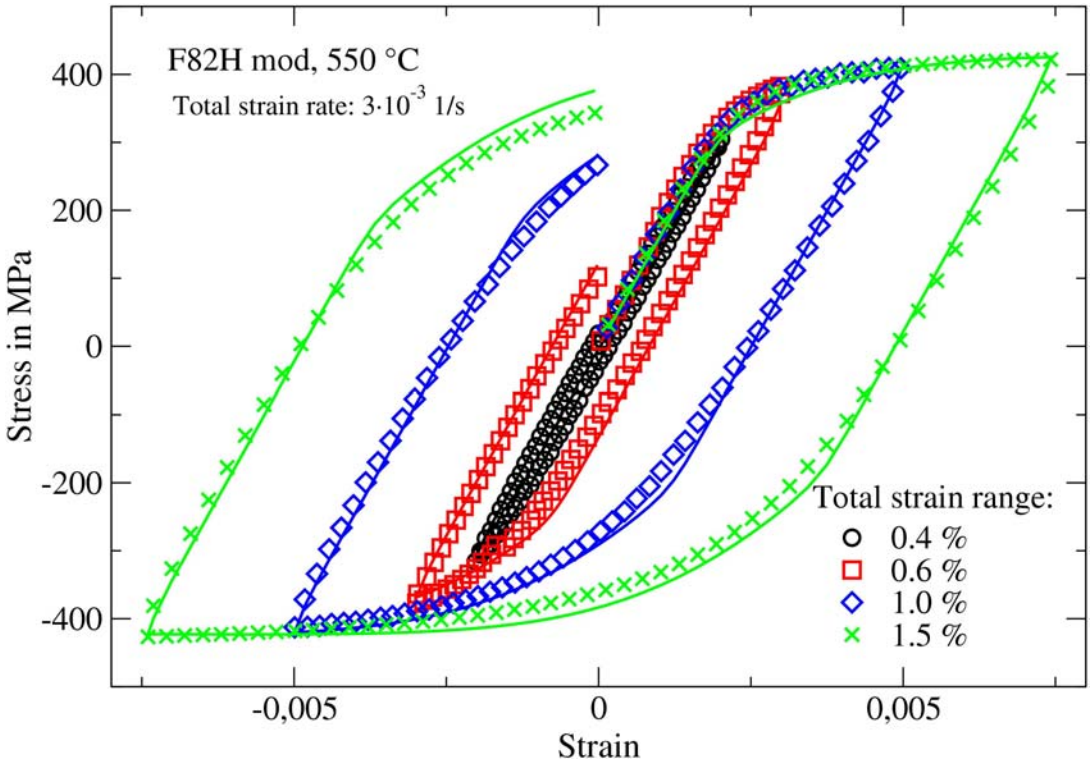


Fig. 4-1 Comparison between material (markers) and model (line) responses for the first stress strain hysteresis of strain controlled LCF tests performed with different total strain ranges

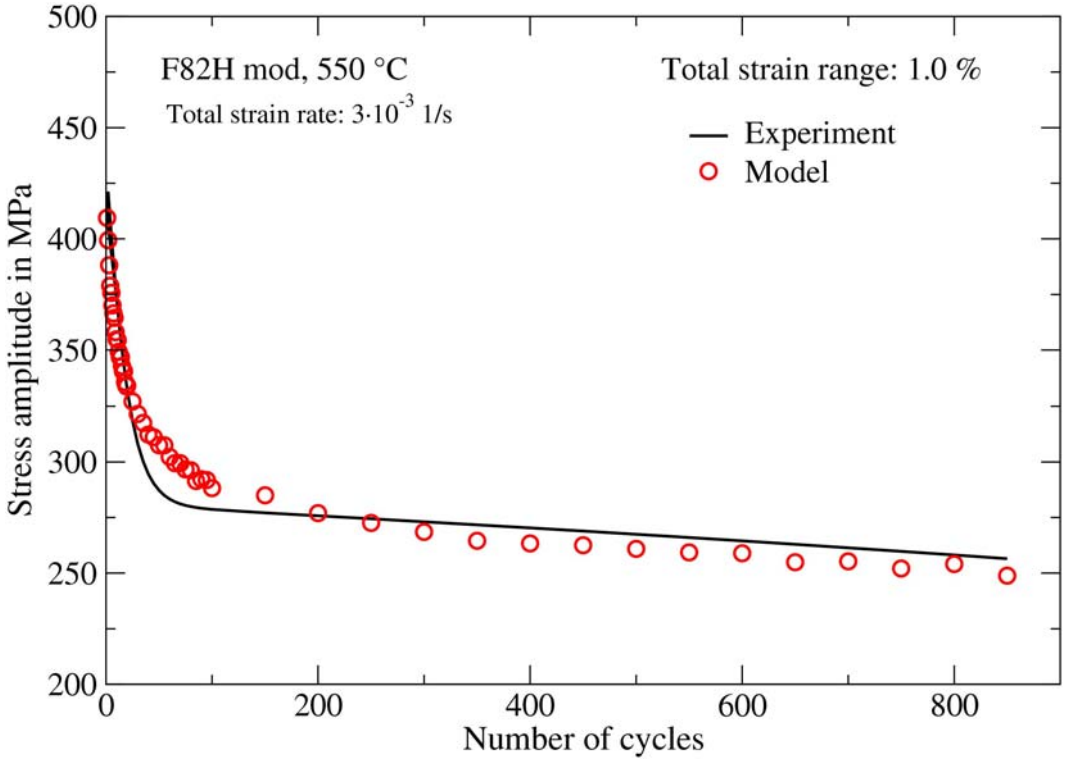


Fig. 4-2 Comparison between material (markers) and model (line) responses for the variation of stress amplitude versus the number of cycles of a strain controlled LCF test

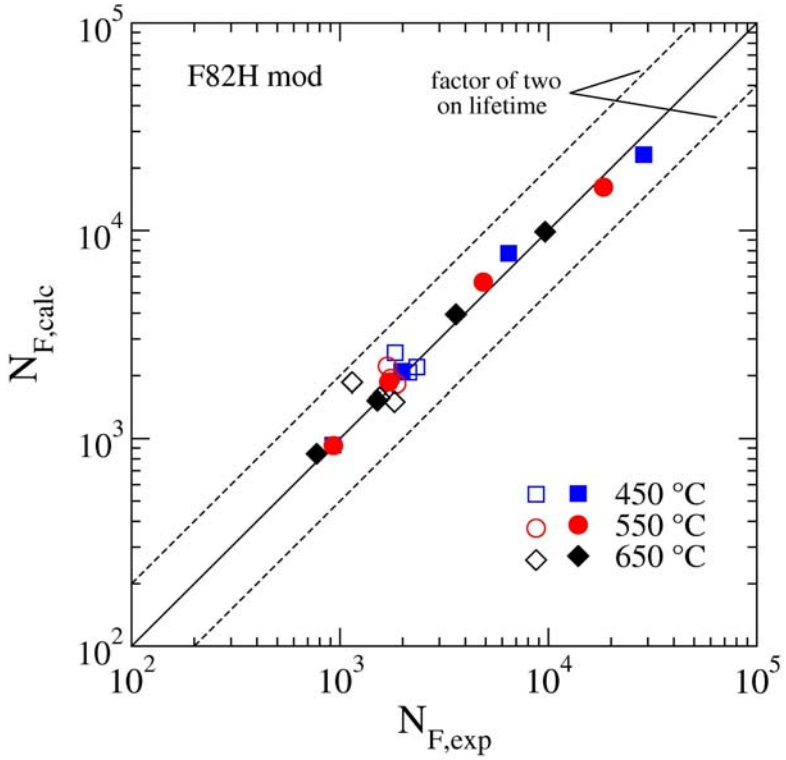


Fig. 4-3 Comparison between numbers of cycles to failure calculated by the coupled deformation damage model with those determined experimentally for F82H mod in LCF tests without (solid symbols) and with hold time (open symbols)

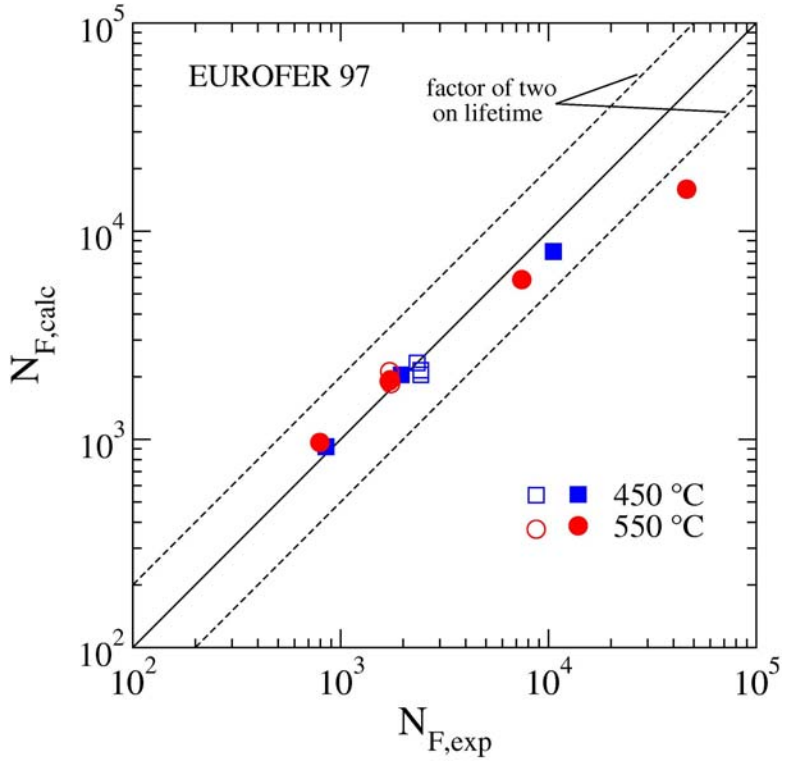


Fig. 4-4 Comparison between numbers of cycles to failure calculated by the coupled deformation damage model with those determined experimentally for EUROFER97 in LCF tests without (solid symbols) and with hold time (open symbols)

In first verifications the fitted model was applied to predict the lifetimes of the LCF tests with hold time. Also there good results are obtained (s. Figs. 4-3 and 4-4).

The results obtained so far give a great hope that the developed model will be able to predict the material behaviour of RAFM steels under fusion reactor loading conditions what has to be verified in further applications to:

1. isothermal two-steps LCF-tests (low-to-high and high-to-low) - to verify the assumption of the linear accumulation of damage

2. thermo-mechanical LCF-tests - because the loading in the First Wall of a fusion reactor is mainly of this type

3. isothermal multi-axial LCF-tests - because the loading in a fusion reactor is multi-axial

4. as well as to a suitable mock-up test.

In addition, the influence of irradiation which is in a first approach implemented in the model assuming a dependence of the model parameters on the irradiation dose, needs extensive investigations starting with applications of the model to several irradiated states which require sufficient data base for the selected RAFM steels in different irradiated states to be available.

# 5 Literature

[1] B. van der Schaaf, F. Tavassoli, C. Fazio, E. Rigal, E. Diegele, R. Lindau and G. LeMarois, The development of EUROFER reduced activation steel, Fusion Engineering and Design, Volume 69, Issues 1-4, September 2003, Pages 197-203.

[2] E. Diegele, D. Munz and G. Rizzi, Design and life assessment of first wall components, Fusion Engineering and Design, Volume 27, 1 March 1995, Pages 210-215.

[3] E. Diegele, R. Krüssmann, S. Malang, P. Norajitra and G. Rizzi, Modular He-cooled divertor for power plant application, Fusion Engineering and Design, Volumes 66-68, September 2003, Pages 383-387.

[4] Chaboche, J.L., Viscoplastic Constitutive Equations for the Description of Cyclic and Anisotropic Behaviour of Metals, Bull. de l'Acad. Polonaise des Sciences, Sc. et Tech., 25(1), (1977), pp. 33-42.

[5] Walker, K.P., Research and Development for Nonlinear Structural Modelling with Advanced Time-Temperature Dependent Constitutive Relationships, NASA CR-165533, (1981).

[6] J. Aktaa and B. Schinke, The influence of the hardening state on time dependent damage and its consideration in a unified damage model, Fatigue Engng Mater. Struct., vol. 19, pp. 1143-1151, 1996.

[7] J. Aktaa, M. G. Horsten and R. Schmitt, Effects of hold-time and neutron-irradiation on the low-cycle fatigue behaviour of type 316-CL and their consideration in a damage model, Nuclear Engineering and Design, 213 (2002) 111-117.

[8] Kachanov, L.M., Time of the rupture process under creep conditions, TVZ Akad. Nauk. S.S.R. Otd. Tech. Nauk., vol.8, (1958).

[9] Lemaitre, J.: Evaluation of dissipation and damage in metals submitted to dynamic loading, Proc. I.C.M. 1, Kyoto, Japan, (1971).

[10] J. Aktaa, Kontinuumsmechanische Modellierung der zeitabhängigen Schädigung bei hohen Temperaturen, Dissertation, Universität Karlsruhe, Fortschr. -Ber. VDI Reihe 20 Nr. 144. Düsseldorf: VDI-Verlag 1994.

[11] J. Aktaa and D. Munz, Modeling of the non-linear deformation and damage behaviour of combustor structure materials, in "High Intensity Combustors- Steady Isobaric Combustion," eds. S. Wittig, O. Vöhringer and S. Kim, WILEY-VCH Verlag, 2002, pp. 391-416.

# Appendix A Multiaxial formulation of the coupled deformation damage model

$$\dot{\boldsymbol{\varepsilon}} = \dot{\boldsymbol{\varepsilon}}^{el} + \dot{\boldsymbol{\varepsilon}}^{in} + \dot{\boldsymbol{\varepsilon}}^{th}$$

$$\boldsymbol{\varepsilon}^{th} = \alpha \ (\mathrm{T} - \mathrm{T}_0) \ \mathbf{1}$$

$$\boldsymbol{\varepsilon}^{el} = (1 - D) \ \mathbf{E} : \boldsymbol{\sigma}$$

$$\dot{\boldsymbol{\varepsilon}}^{in} = \frac{3}{2} \left\langle \frac{\Sigma_{eq} - k}{Z} \right\rangle^{n} \frac{\boldsymbol{\Sigma}}{\Sigma_{eq}} \quad \text{with} \quad \boldsymbol{\Sigma} = \frac{\mathbf{s}}{\psi(1 - \mathrm{D})} - \boldsymbol{\Omega} \quad \text{and} \quad \Sigma_{eq} = \sqrt{\frac{3}{2} \mathbf{s} : \mathbf{s}}$$

$$\dot{\boldsymbol{\Omega}} = \frac{2}{3} H \ \dot{\boldsymbol{\varepsilon}}^{in} - D \ \boldsymbol{\Omega} \ \dot{\mathrm{p}} - R \ |\boldsymbol{\Omega}|^{m-1} \boldsymbol{\Omega} \quad \text{with} \quad \dot{\mathrm{p}} = \sqrt{\frac{2}{3} \dot{\boldsymbol{\varepsilon}}^{in} : \dot{\boldsymbol{\varepsilon}}^{in}}$$

$$\psi = \psi_1 + \psi_2 \quad \text{with} \quad \psi_1 (\mathrm{t} = 0) = 0 \quad \text{and} \quad \psi_2 (\mathrm{t} = 0) = 1$$

$$\dot{\psi}_1 = -h \ \dot{\mathrm{p}}$$

$$\dot{\psi}_2 = c \ (\psi_s - \psi_2) \dot{\mathrm{p}} - r_{\psi} |\psi_2 - \psi_r|^{m_{\psi} - 1} (\psi_2 - \psi_r)$$

$$\text{with} \quad \psi_s = 1 - \psi_{s,\infty} \left( 1 - \exp\left( - c_s \max_{-\infty < \tau < t} \varepsilon_{eq}^{in}(\tau) \right) \right) \quad \text{and} \quad \varepsilon_{eq}^{in}(\tau) = \sqrt{\frac{2}{3} \boldsymbol{\varepsilon}^{in}(\tau) : \boldsymbol{\varepsilon}^{in}(\tau)}$$

$$\dot{\mathrm{D}} = \left\langle \frac{\chi(\boldsymbol{\sigma})}{A} \right\rangle^{r} \dot{\mathrm{p}} \ (1 - \mathrm{D})^{-\kappa}$$

$$\text{with} \quad \chi(\boldsymbol{\sigma}) = \alpha_1 \sigma_1 + \alpha_2 \mathrm{Trace}(\boldsymbol{\sigma}) + (1 - \alpha_1 - \alpha_2) \sigma_{eq}$$

*whereas* $\sigma_1 \hat{=} \text{maximum principle stress}$ and $\sigma_{eq} = \sqrt{\frac{3}{2} \mathbf{s} : \mathbf{s}}$

$\mathbf{s}$ is the deviatoric part of the stress tensor: $\mathbf{s} = \boldsymbol{\sigma} - \frac{1}{3} \mathrm{Trace}(\boldsymbol{\sigma}) \mathbf{1}$

$\alpha_1$ and $\alpha_2$ are additional material, temperature and irradiation dose dependent parameters needed for the use of the model in the multi-axial case. They can be determined using life-time data from multi-axial experiments.

# Appendix B Determined parameters of the coupled deformation damage model

| Material | **F82H mod** | | | **EUROFER 97** | |
|---|---|---|---|---|---|
| Temperature [°C] | 450 | 550 | 650 | 450 | 550 |
| $E$ [MPa] | 176170 | 160000 | 137450 | 166300 | 153890 |
| $k$ [MPa] | 5.57 | $1.3\cdot10^{-6}$ | $2.14\cdot10^{-5}$ | 175 | $6\cdot10^{-6}$ |
| $Z$ [MPa·s$^{1/n}$] | 391.6 | 524 | 600 | 177.6 | 428 |
| $n$ | 31.8 | 11.7 | 6.66 | 13.7 | 12.57 |
| $H$ [MPa] | 104823 | 78708 | 75646 | 115508 | 98391 |
| $D$ | 619 | 692 | 1046 | 704 | 764 |
| $R$ [MPa$^{1-m}$·s$^{-1}$] | $1.0\cdot10^{-21}$ | $9.9\cdot10^{-17}$ | $8\cdot10^{-17}$ | $4\cdot10^{-17}$ | $1\cdot10^{-16}$ |
| $m$ | 8.67 | 0.428 | 0.397 | 6.1 | 0.428 |
| $h$ | $1.7\cdot10^{-3}$ | $1.87\cdot10^{-3}$ | $4.25\cdot10^{-3}$ | $1.85\cdot10^{-5}$ | $9.8\cdot10^{-4}$ |
| $c$ | 6.3 | 5.02 | 6.21 | 1.82 | 3.62 |
| $r_\psi$ [s$^{-1}$] | $8.27\cdot10^{-5}$ | $1.03\cdot10^{-4}$ | $2\cdot10^{-5}$ | $7\cdot10^{-5}$ | $1\cdot10^{-4}$ |
| $\psi_r$ | 0.501 | 0.519 | $1\cdot10^{-4}$ | 0.622 | 0.542 |
| $m_\psi$ | 1.0 | 1.0 | 1.0 | 1.0 | 1.0 |
| $\psi_{s,\infty}$ | 0.308 | 0.346 | 0.377 | 0.293 | 0.35 |
| $c_s$ | 2452 | 3000 | 2814 | 2764 | 2507 |
| $A$ [MPa·s$^{1/r}$] | 2293 | 1592 | 1391 | 2202 | 2057 |
| $r$ | 2.91 | 2.64 | 2.34 | 2.91 | 2.25 |
| $\kappa$ | 33.51 | 12.64 | 12.44 | 33.51 | 12.25 |

# Appendix C Comparisons between experiment and model

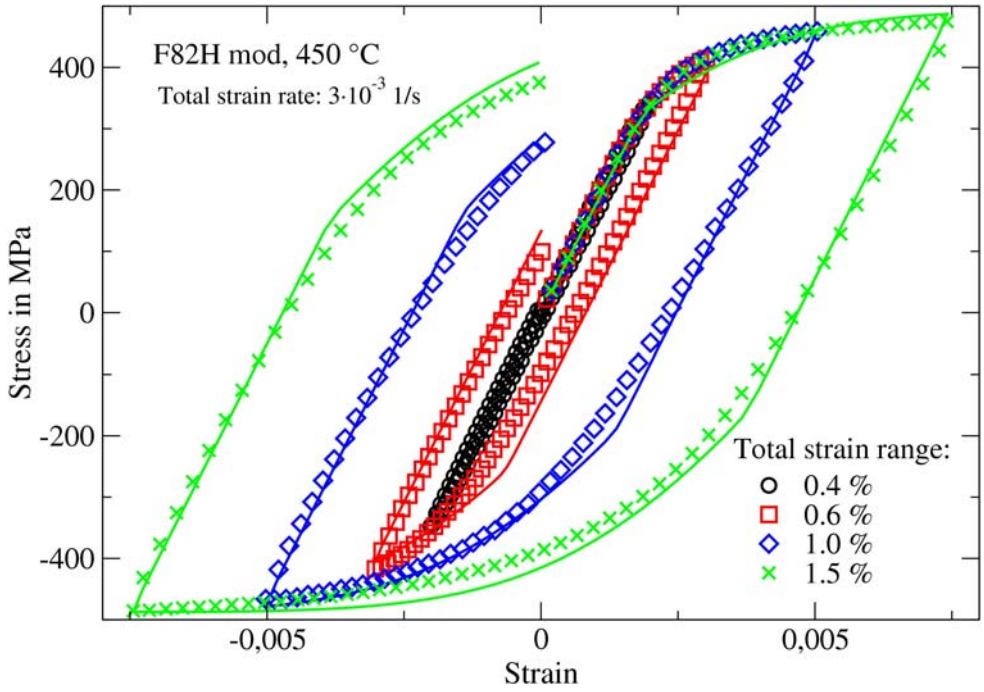


Fig. 4-5 Comparison between material (markers) and model (line) responses for the first stress strain hysteresis of strain controlled LCF tests performed with different total strain ranges

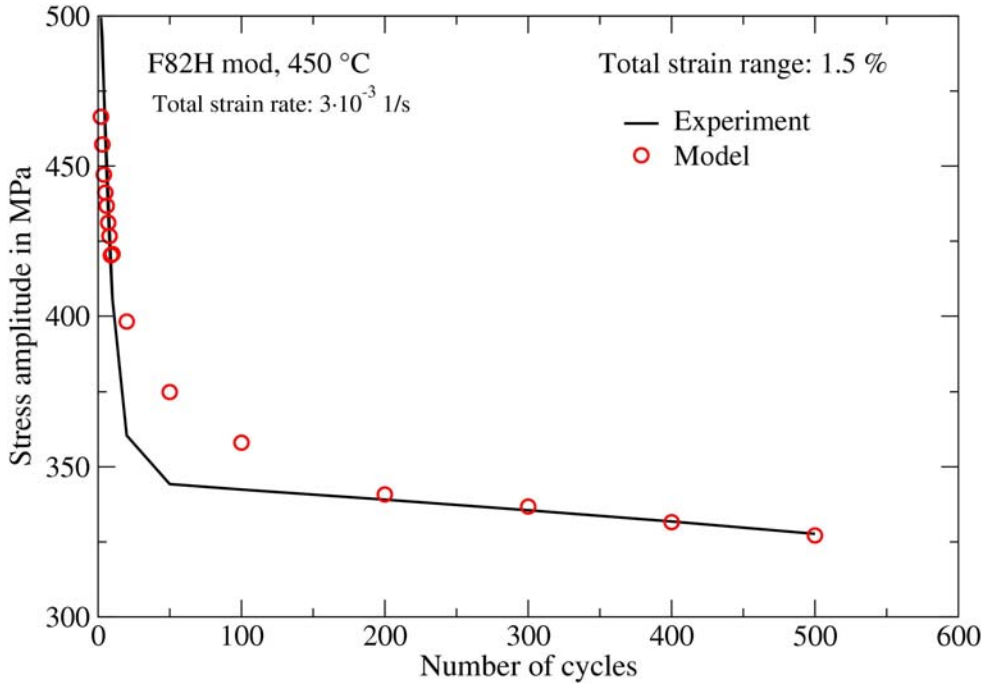


Fig. 4-6 Comparison between material (markers) and model (line) responses for the variation of stress amplitude versus the number of cycles of a strain controlled LCF test

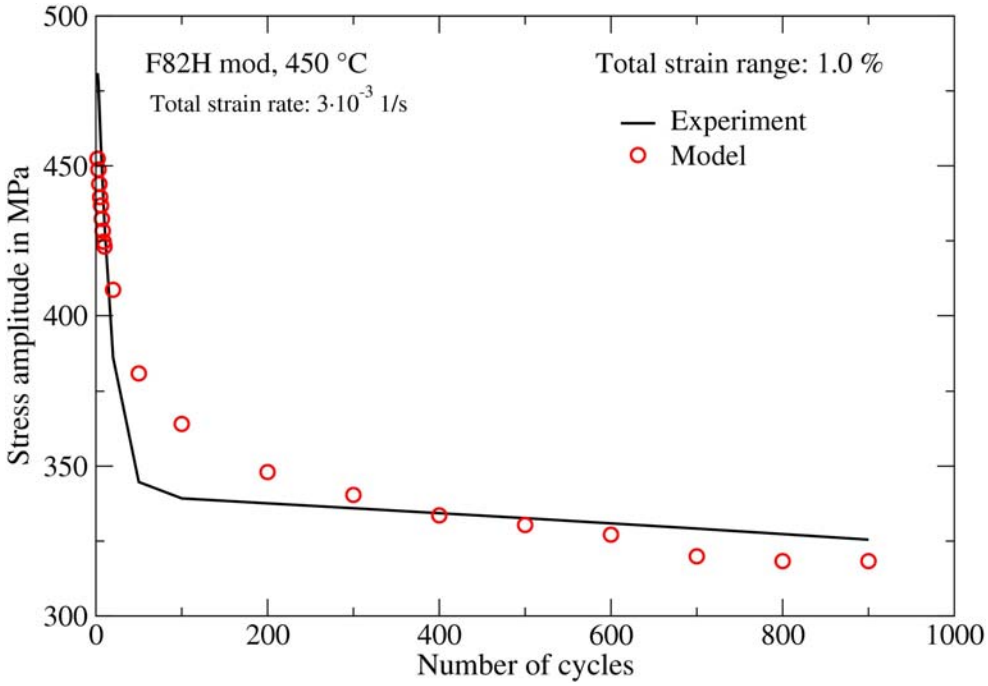


Fig. 4-7 Comparison between material (markers) and model (line) responses for the variation of stress amplitude versus the number of cycles of a strain controlled LCF test

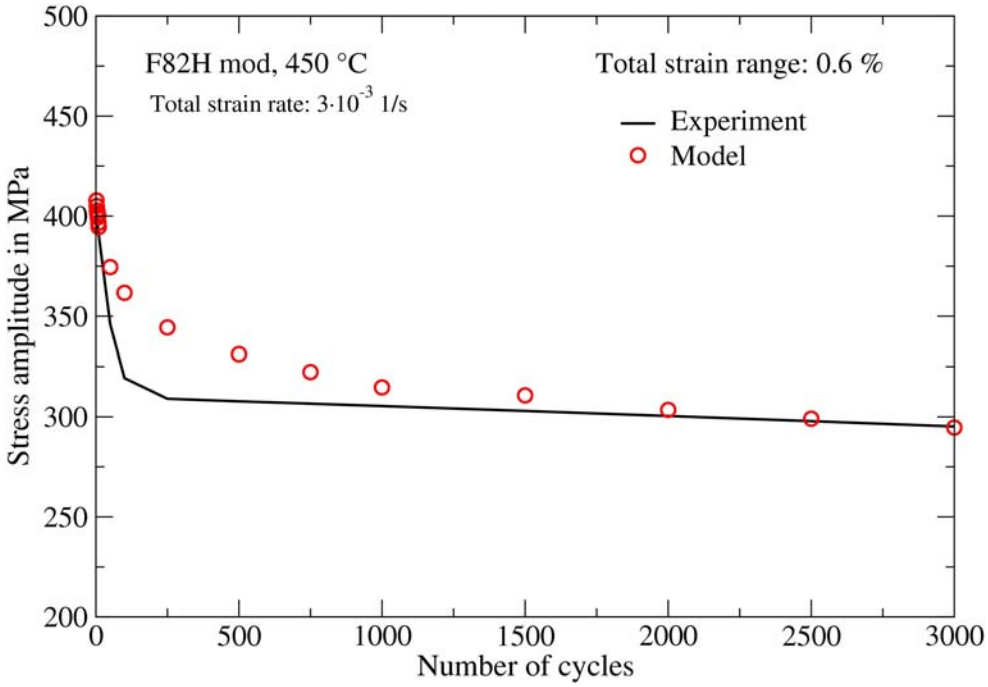


Fig. 4-8 Comparison between material (markers) and model (line) responses for the variation of stress amplitude versus the number of cycles of a strain controlled LCF test

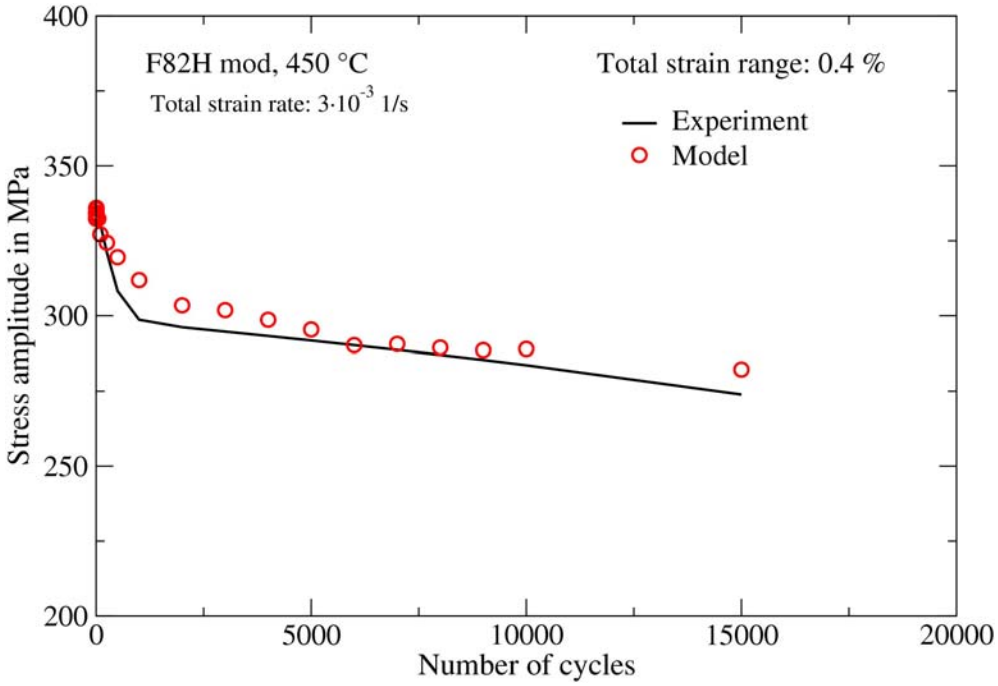


Fig. 4-9 Comparison between material (markers) and model (line) responses for the variation of stress amplitude versus the number of cycles of a strain controlled LCF test

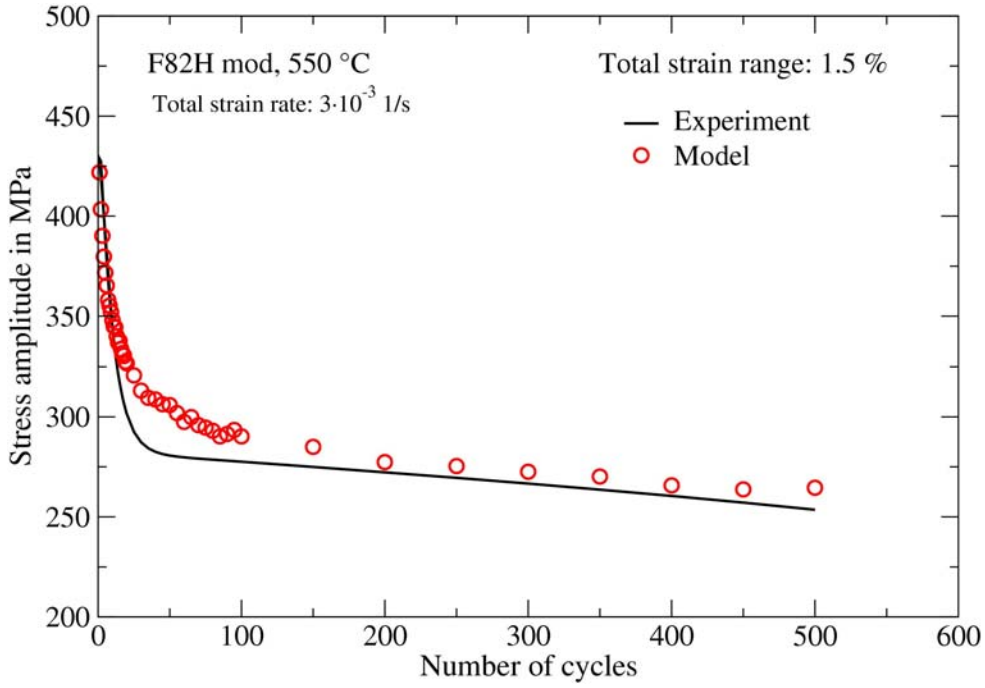


Fig. 4-10 Comparison between material (markers) and model (line) responses for the variation of stress amplitude versus the number of cycles of a strain controlled LCF test

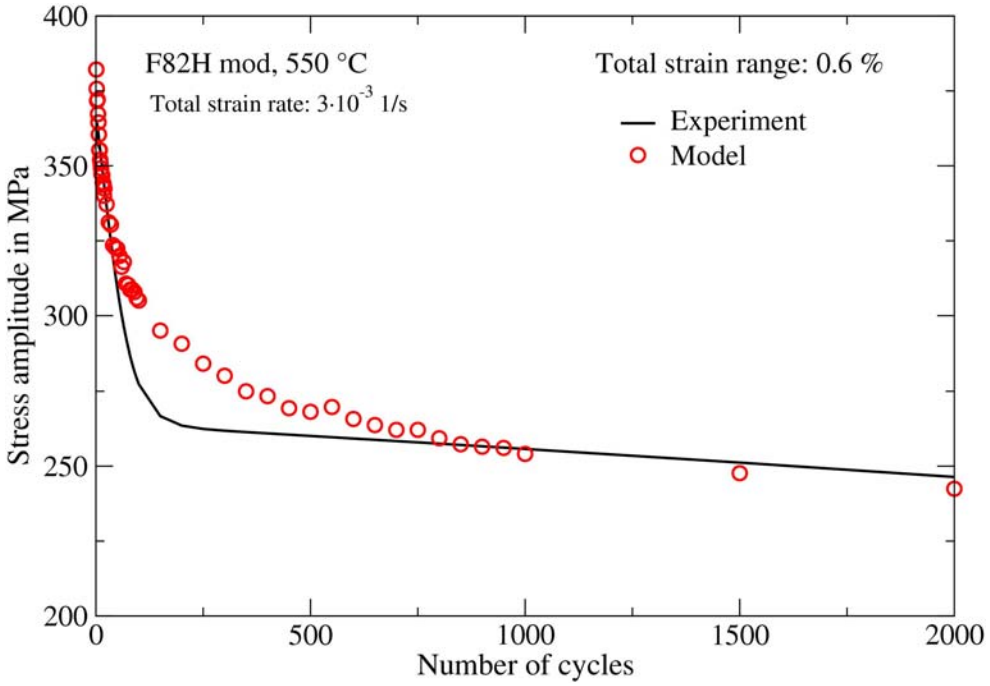


Fig. 4-11 Comparison between material (markers) and model (line) responses for the variation of stress amplitude versus the number of cycles of a strain controlled LCF test

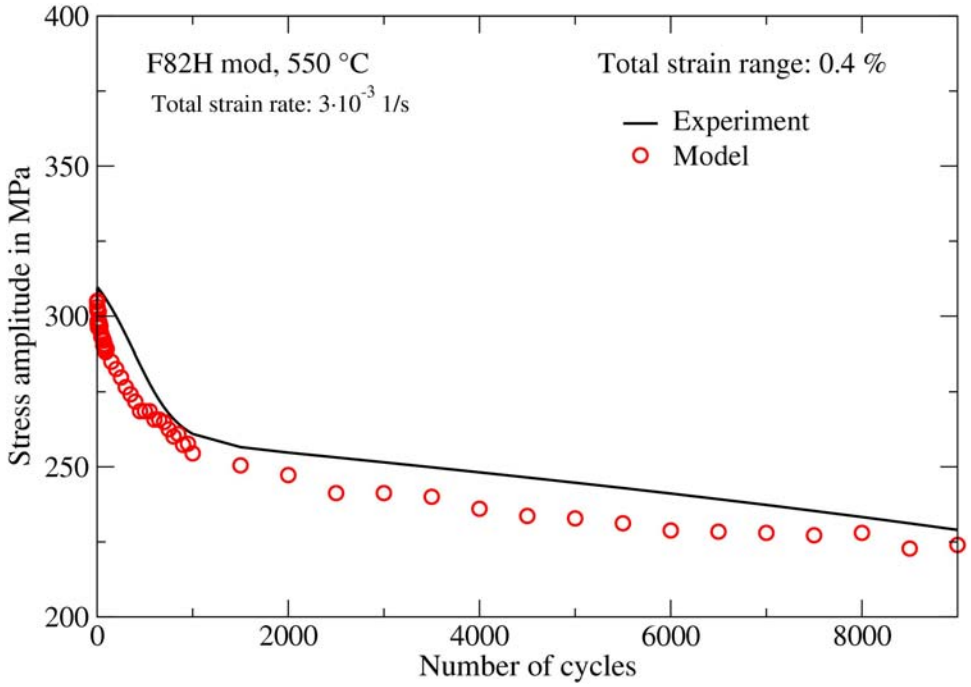


Fig. 4-12 Comparison between material (markers) and model (line) responses for the variation of stress amplitude versus the number of cycles of a strain controlled LCF test

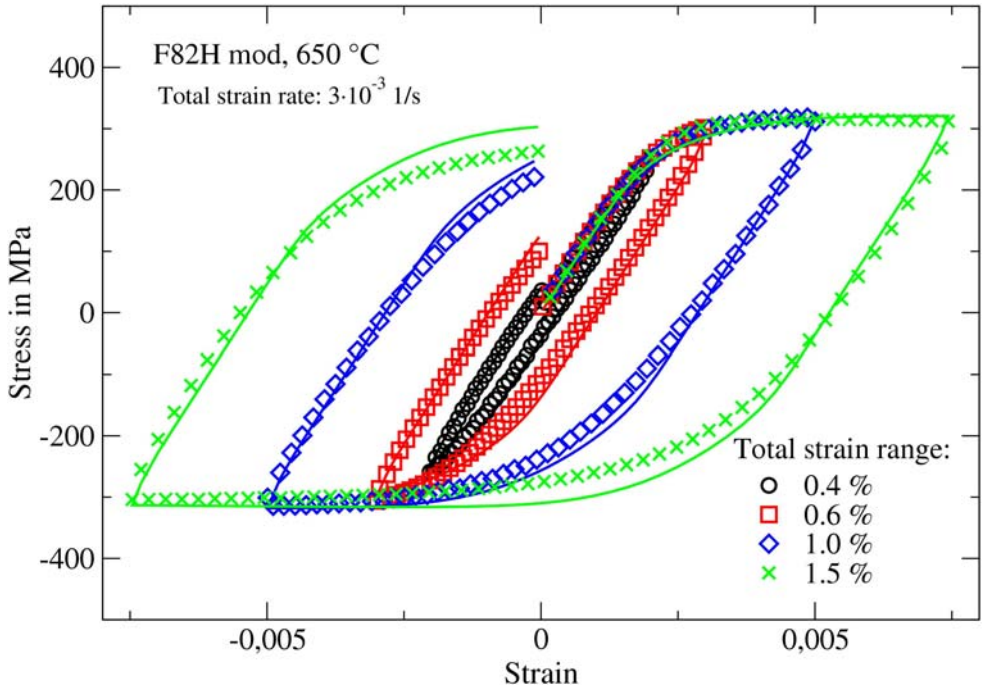


Fig. 4-13 Comparison between material (markers) and model (line) responses for the first stress strain hysteresis of strain controlled LCF tests performed with different total strain ranges

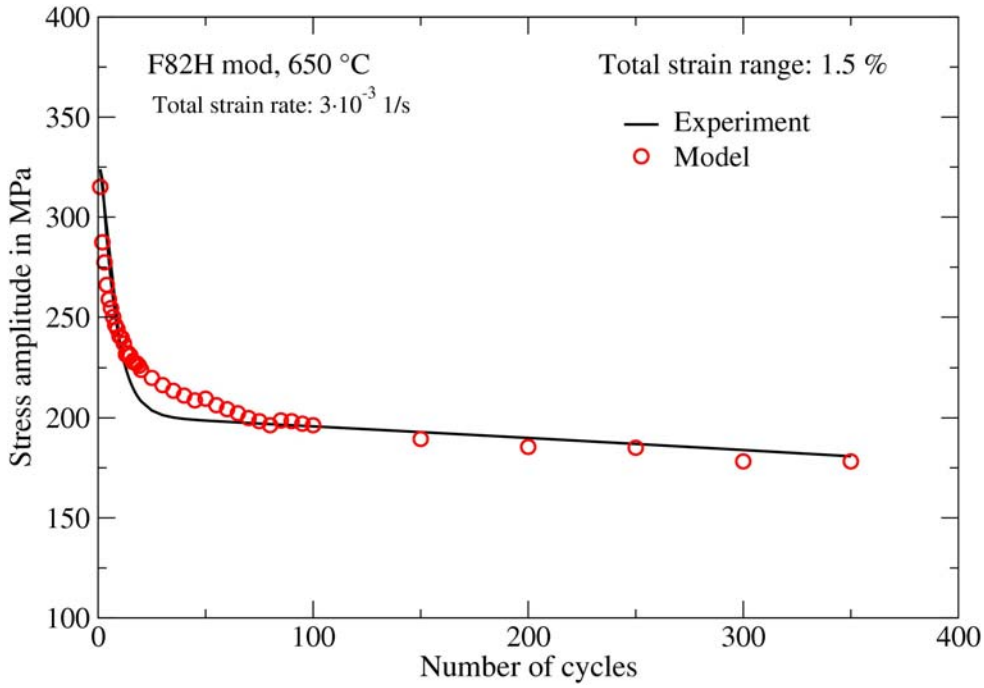


Fig. 4-14 Comparison between material (markers) and model (line) responses for the variation of stress amplitude versus the number of cycles of a strain controlled LCF test

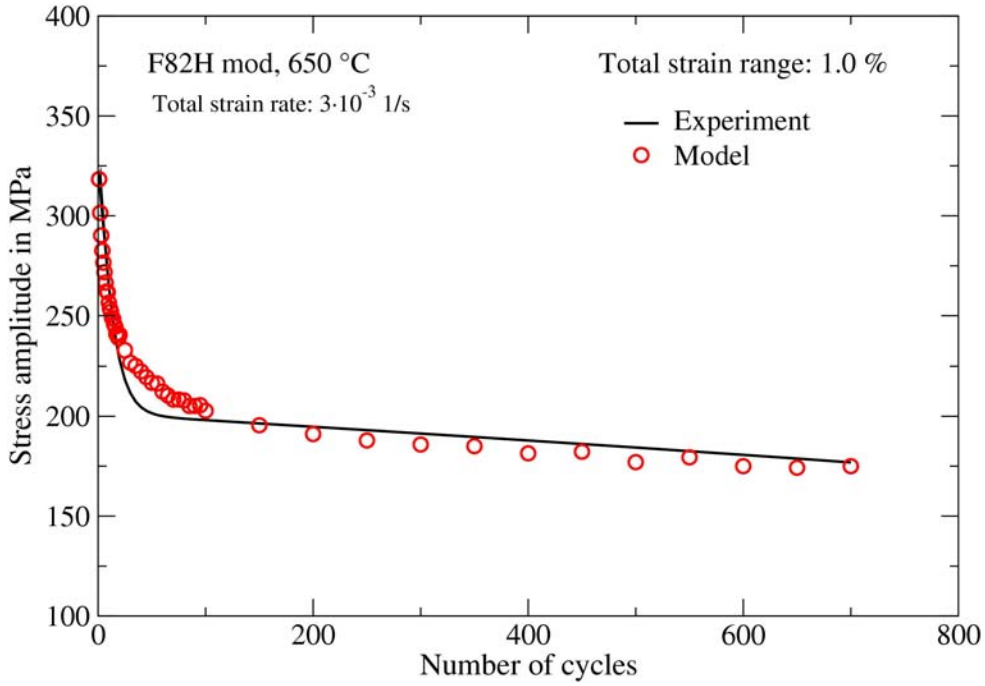


Fig. 4-15 Comparison between material (markers) and model (line) responses for the variation of stress amplitude versus the number of cycles of a strain controlled LCF test

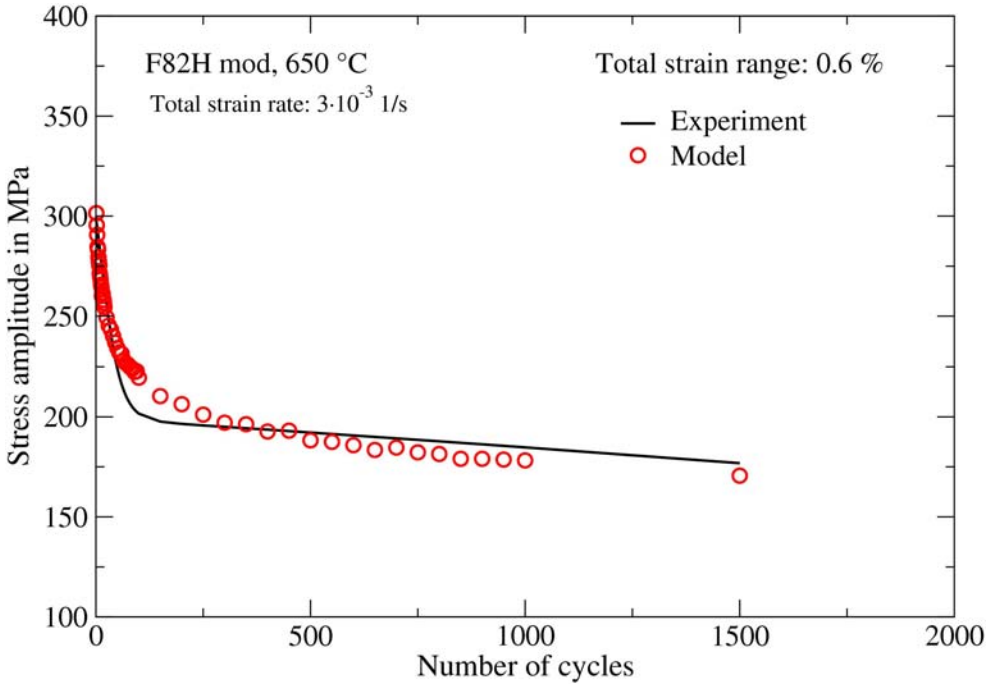


Fig. 4-16 Comparison between material (markers) and model (line) responses for the variation of stress amplitude versus the number of cycles of a strain controlled LCF test

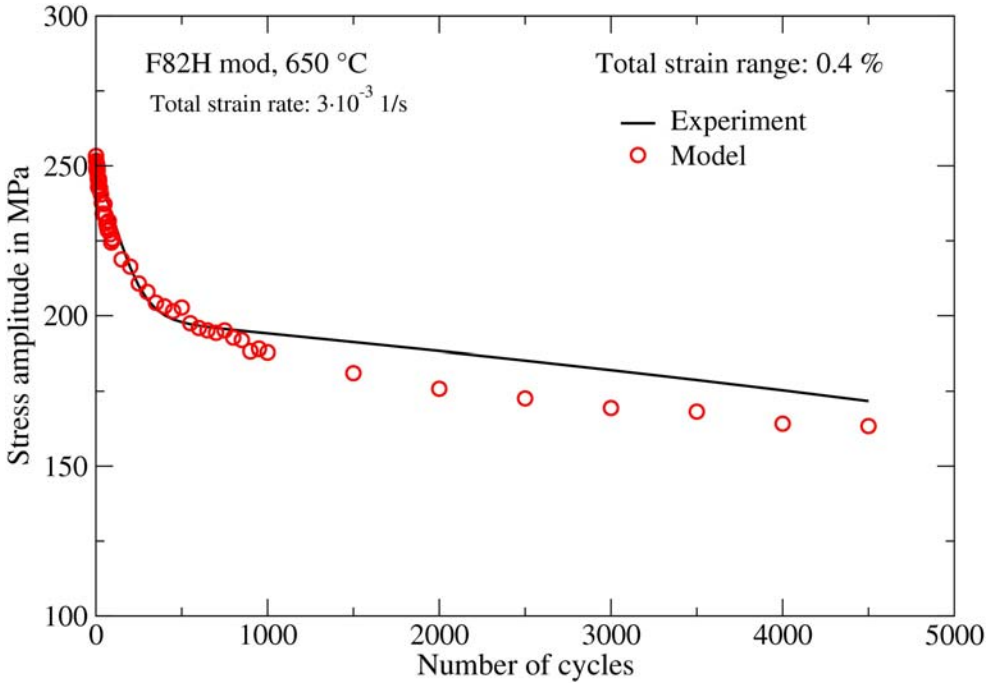


Fig. 4-17 Comparison between material (markers) and model (line) responses for the variation of stress amplitude versus the number of cycles of a strain controlled LCF test

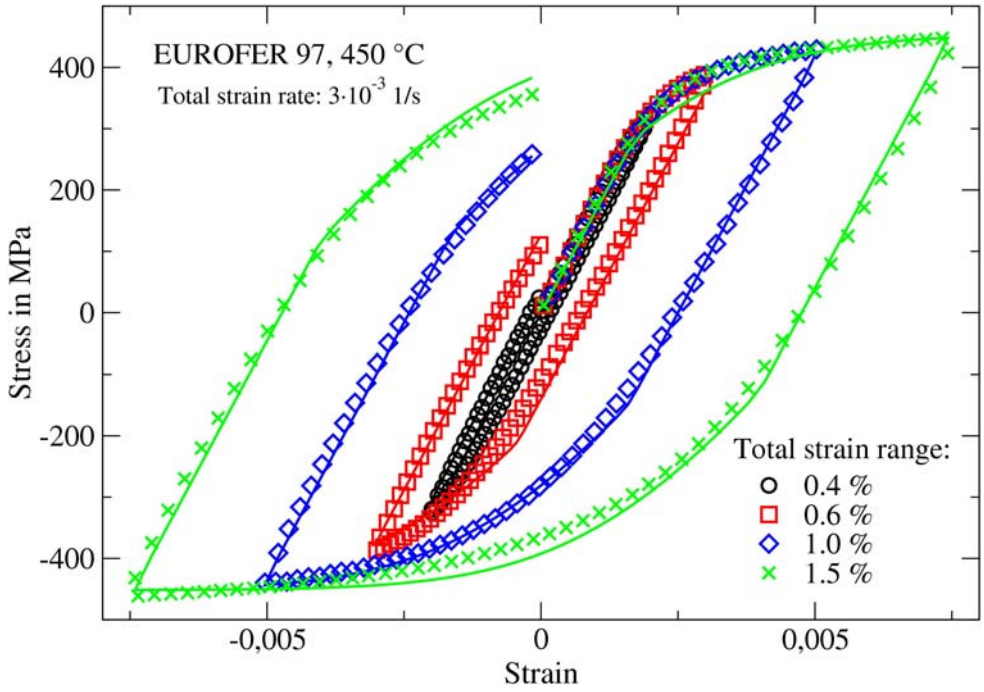


Fig. 4-18 Comparison between material (markers) and model (line) responses for the first stress strain hysteresis of strain controlled LCF tests performed with different total strain ranges

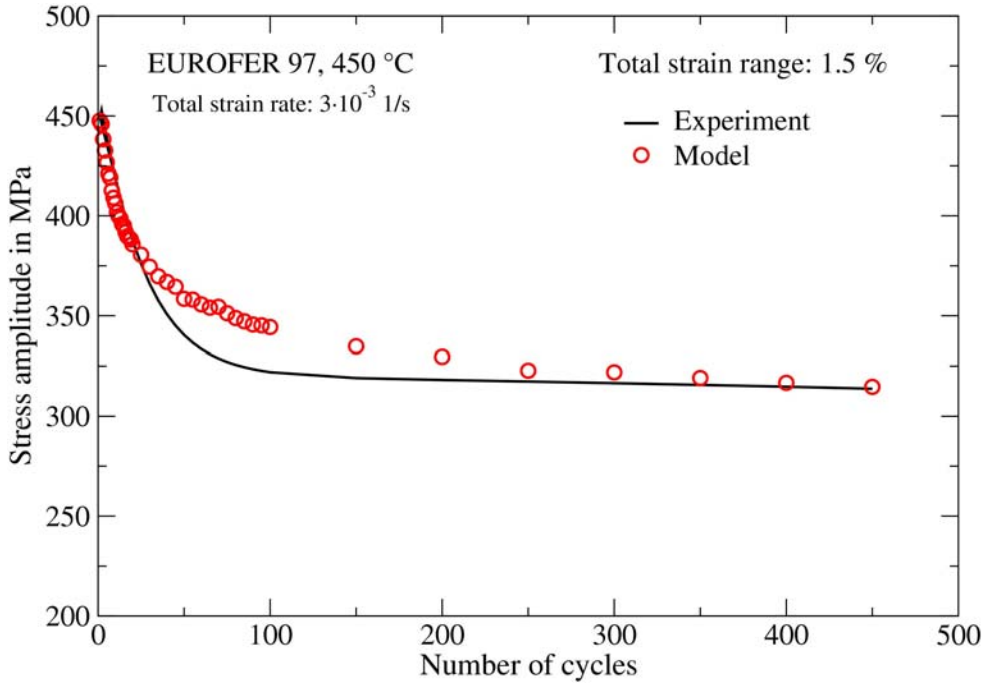


Fig. 4-19 Comparison between material (markers) and model (line) responses for the variation of stress amplitude versus the number of cycles of a strain controlled LCF test

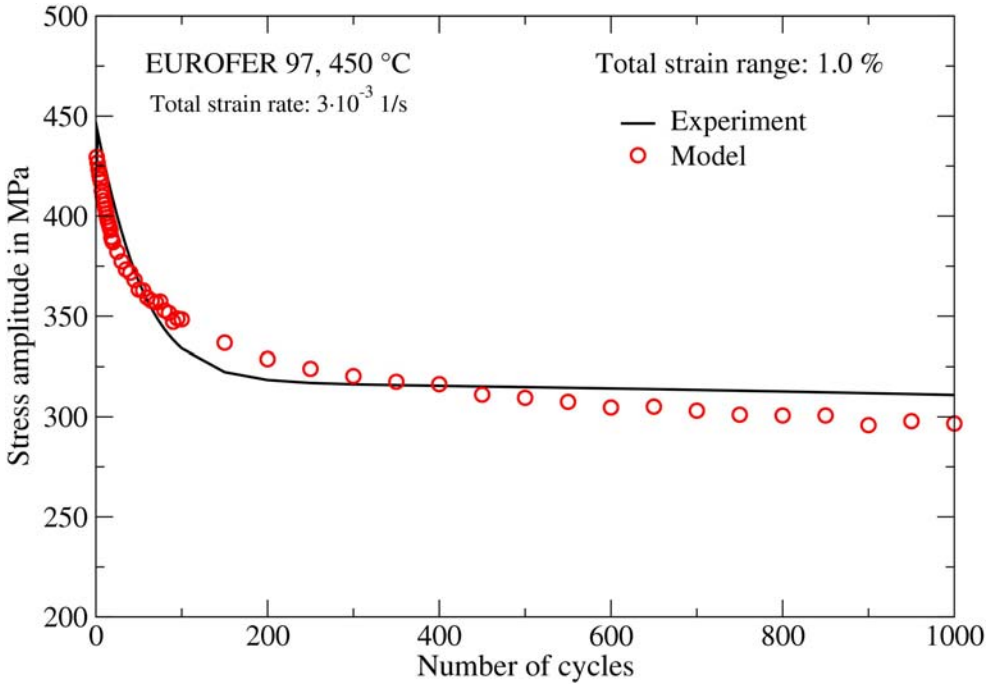


Fig. 4-20 Comparison between material (markers) and model (line) responses for the variation of stress amplitude versus the number of cycles of a strain controlled LCF test

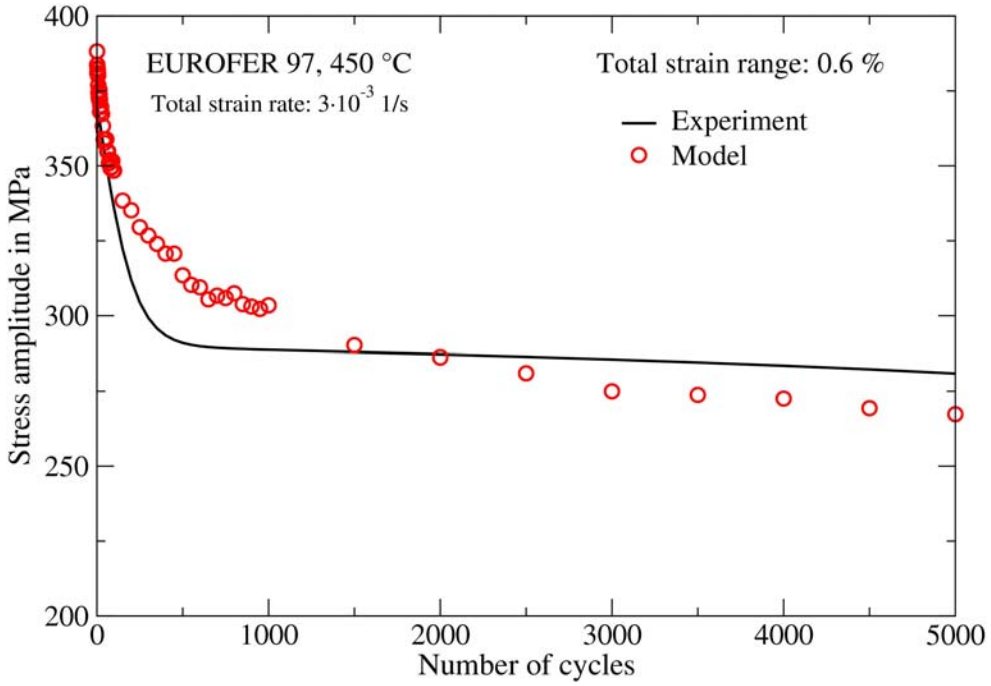


Fig. 4-21 Comparison between material (markers) and model (line) responses for the variation of stress amplitude versus the number of cycles of a strain controlled LCF test

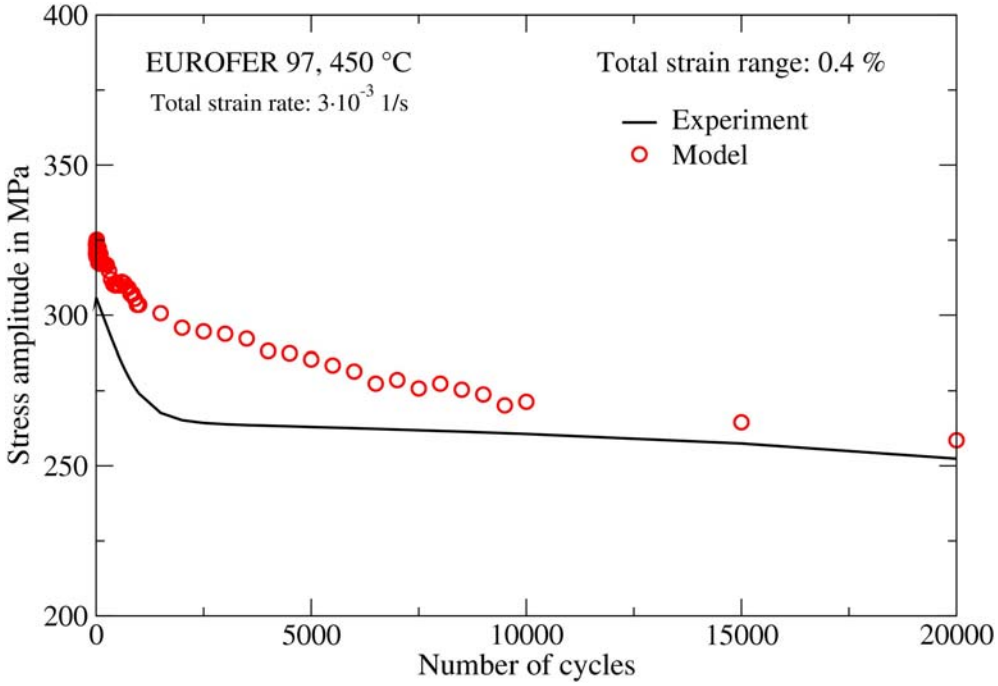


Fig. 4-22 Comparison between material (markers) and model (line) responses for the variation of stress amplitude versus the number of cycles of a strain controlled LCF test

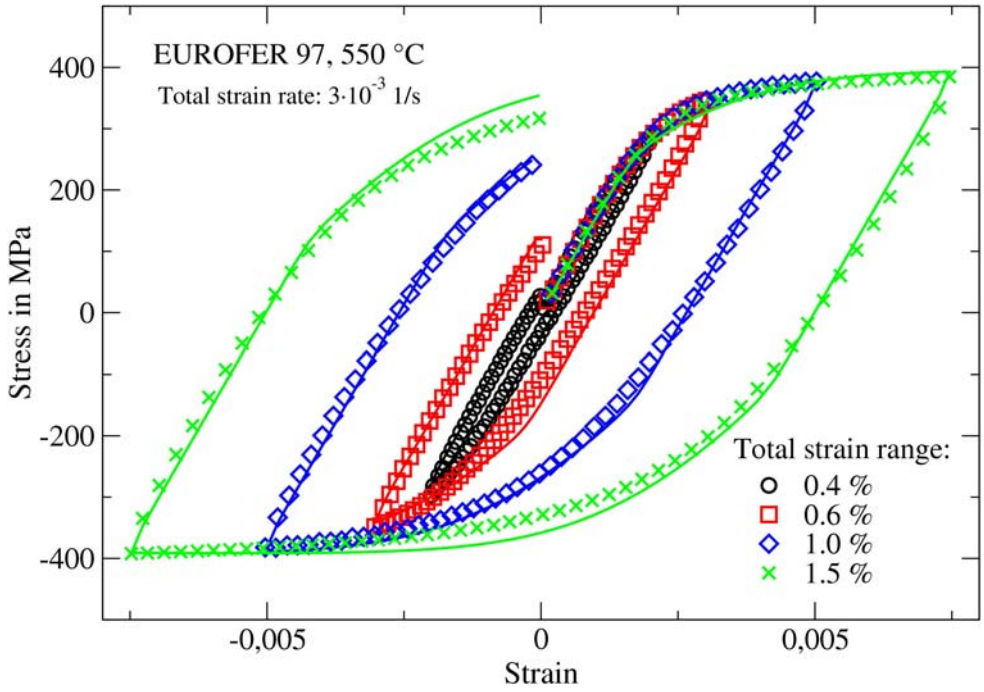


Fig. 4-23 Comparison between material (markers) and model (line) responses for the first stress strain hysteresis of strain controlled LCF tests performed with different total strain ranges

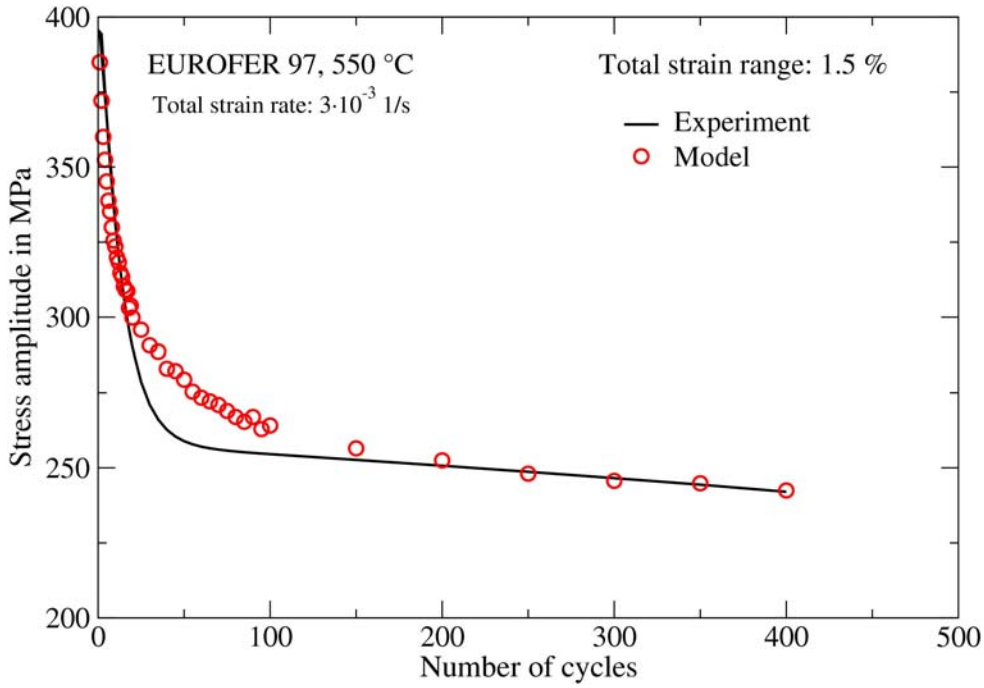


Fig. 4-24 Comparison between material (markers) and model (line) responses for the variation of stress amplitude versus the number of cycles of a strain controlled LCF test

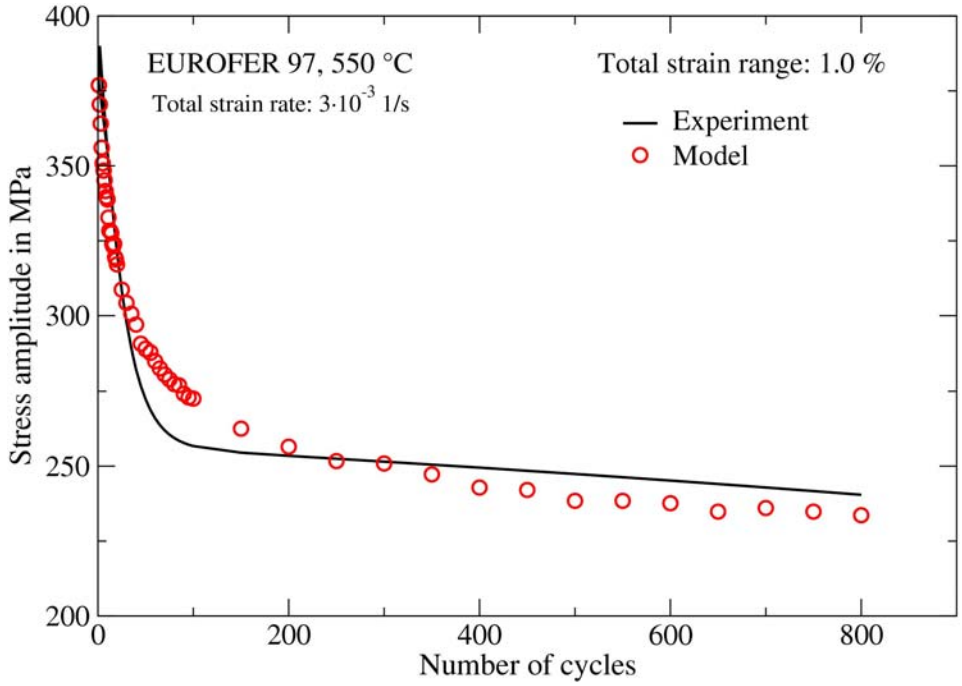


Fig. 4-25 Comparison between material (markers) and model (line) responses for the variation of stress amplitude versus the number of cycles of a strain controlled LCF test

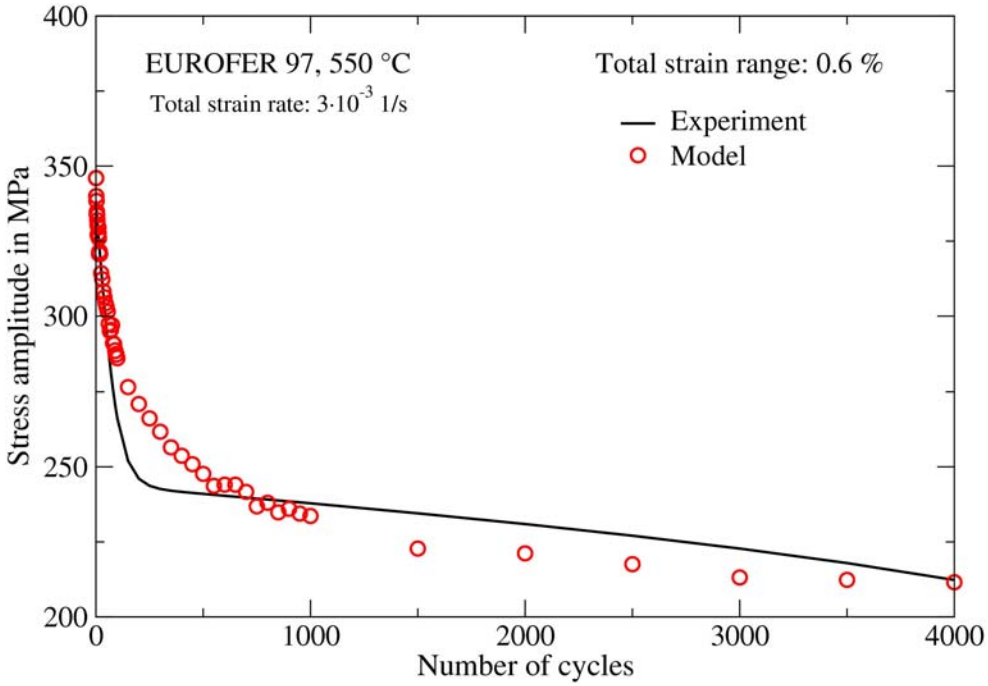


Fig. 4-26 Comparison between material (markers) and model (line) responses for the variation of stress amplitude versus the number of cycles of a strain controlled LCF test

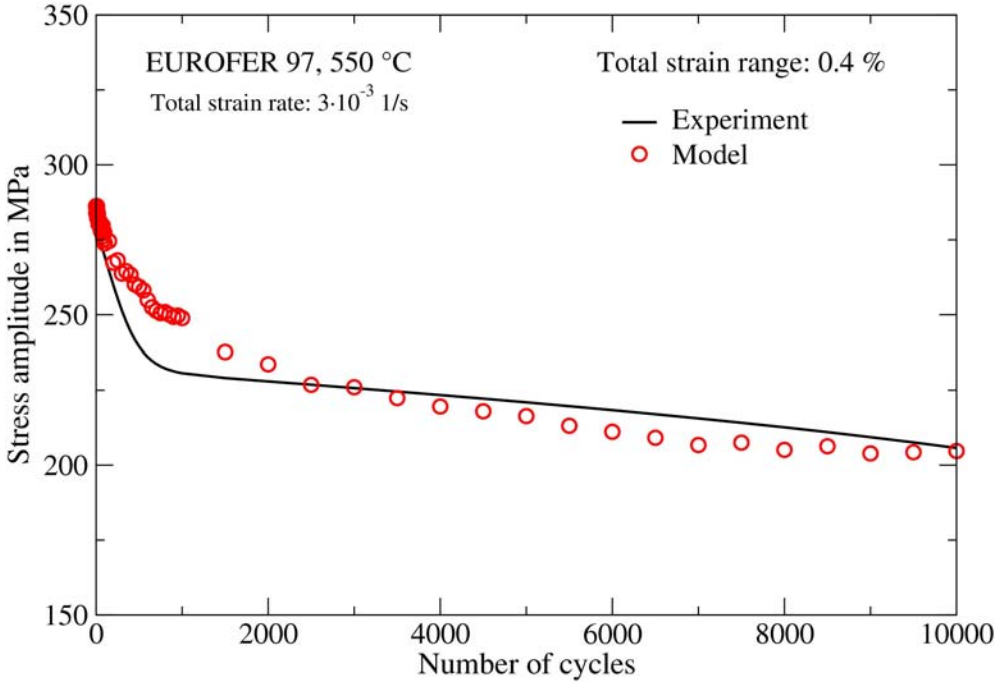


Fig. 4-27 Comparison between material (markers) and model (line) responses for the variation of stress amplitude versus the number of cycles of a strain controlled LCF test